

# Calcineurin-mediated intracellular organelle calcium homeostasis is required for the survival of fungal pathogens upon extracellular calcium stimuli

Chi Zhang, Yiran Ren, Huiyu Gu, Lu Gao, Yuanwei Zhang , and Ling Lu 

Jiangsu Key Laboratory for Microbes and Functional Genomics, Jiangsu Engineering and Technology Research Centre for Microbiology, College of Life Sciences, Nanjing Normal University, Nanjing, China

## ABSTRACT

In eukaryotes, calcium not only is an essential mineral nutrient but also serves as an intracellular second messenger that is necessary for many physiological processes. Previous studies showed that the protein phosphatase-calcineurin protects fungi from toxicity caused by the extracellular calcium; however, little is known about how calcineurin mediates the cellular physiology process for this function. In this study, by monitoring intracellular calcium, particularly by tracking vacuolar calcium dynamics in living cells through a novel procedure using modified aequorin, we found that calcineurin dysfunction systematically caused abnormal intracellular calcium homeostasis in cytosol, mitochondria, and vacuole, leading to drastic autophagy, global organelle fragmentation accompanied with the increased expression of cell death-related enzymes, and cell death upon extracellular calcium stimuli. Notably, all detectable defective phenotypes seen with calcineurin mutants can be significantly suppressed by alleviating a cytosolic calcium overload or increasing vacuolar calcium storage capacity, suggesting toxicity of exogenous calcium to calcineurin mutants is tightly associated with abnormal cytosolic calcium accumulation and vacuolar calcium storage capacity deficiency. Our findings provide insights into how the original recognized antifungal drug target-calcineurin regulates intracellular calcium homeostasis for cell survival and may have important implications for antifungal therapy and clinical drug administration.

## ARTICLE HISTORY

Received 26 September 2020  
Revised 31 December 2020  
Accepted 23 March 2021

## KEYWORDS

Fungi; pathogenic fungi; *aspergillus fumigatus*; calcineurin; calcium homeostasis; autophagy


## Introduction

Calcium ( $\text{Ca}^{2+}$ ), as an intracellular second messenger in eukaryotic cells, plays a critical role in the regulation of various cellular processes including synaptic transmission, secretion, and cytokinesis [1,2]. The intracellular  $\text{Ca}^{2+}$  concentration is strictly and precisely controlled by a sophisticated calcium homeostasis system, which is composed of various calcium channels, calcium pumps, and calcium antiporters [2–4]. Overwhelming evidences demonstrate that calcineurin, the conserved  $\text{Ca}^{2+}$ -calmodulin (CaM) activates protein phosphatase, is a master regulator of intracellular calcium homeostasis in fungi [5]. Calcineurin is required for the regulation of cation homeostasis, morphogenesis, cell-wall integrity, and pathogenesis [6]. However, the mechanism by which calcineurin regulates the optimal  $\text{Ca}^{2+}$  concentrations in the cytosol and in intracellular compartments such as the vacuole and mitochondria remains elusive.

When fungal cells encounter environmental stresses, a transient elevation of cytosolic calcium is induced

primarily through calcium influx systems in the plasma membrane such as the high-affinity calcium uptake Cch1-Mid1 channel complex system [4,7]. Calcium-activated calcineurin then dephosphorylates the transcription factor Crz1, which induces its translocation to the nucleus to regulate gene expression. It has been shown that the free cytosolic calcium concentration ( $[\text{Ca}^{2+}]_c$ ) must be maintained at a low, steady level within a narrow physiological range (50–200 nM) after a sudden increase, peaking within seconds and then sharply decreasing within 30 seconds as the excess cytosolic calcium is transiently transferred to calcium stores including the endoplasmic reticulum (ER), vacuoles, and mitochondria by various calcium pumps and calcium antiporters [4,8–11]. In mammals, the ER, mitochondria, and lysosomes are physically and/or functionally linked [12]. The role of  $\text{Ca}^{2+}$  signaling in mitochondria is to determine cellular survival by controlling basal mitochondrial bioenergetics and by regulating apoptosis. Moreover, the lysosomes can act as a  $\text{Ca}^{2+}$  store for  $\text{Ca}^{2+}$  release into the cytosol, thereby

**CONTACT** Yuanwei Zhang  [ywzhang@njnu.edu.cn](mailto:ywzhang@njnu.edu.cn); Ling Lu  [linglu@njnu.edu.cn](mailto:linglu@njnu.edu.cn)

 Supplemental data for this article can be accessed [here](#).

influencing  $\text{Ca}^{2+}$  homeostasis.  $\text{Ca}^{2+}$  signaling in lysosomes may regulate autophagy to respond to cell damage and cell stress [13]. As a topological equivalent, the vacuole is the primary calcium storage organelle in fungi, containing more than 90% of total cellular calcium [14]. Notably, until now there was no reliable system to probe or detect the  $\text{Ca}^{2+}$  concentration in fungal vacuole, probably due to its low internal pH. Vacuolar  $\text{Ca}^{2+}$  sequestration is performed by the collaboration of  $\text{Ca}^{2+}/\text{H}^{+}$  exchangers in the Vcx family and the P-type ATPase Pmc family [15,16]. In contrast, vacuolar  $\text{Ca}^{2+}$  can be released into the cytosol through the mechanosensitive channel Yvc1 and/or transient receptor protein (TRP) channels [7,17–21]. Several lines of evidence in yeast-like and filamentous fungi indicate that the transcription of Pmc family members is dependent on an activated calcineurin-Crz1/CrzA complex, whereas Vcx1 activity is negatively regulated by the calcineurin complex [7,22–25].

In addition to being a calcium store, the fungal vacuole is responsible for the last step of autophagy. Autophagy is a highly conserved catabolic process that mediates the self-degradation of intracellular material, such as proteins, lipids, or even entire organelles. In the conserved autophagy pathway, the double-membrane autophagosome (AP) engulfs cellular components to be delivered for degradation in the lysosome/vacuole [26,27]. Autophagy exists at a basal level in all living cells, but it can be induced in response to various factors such as nitrogen starvation, oxidative stress, ER stress, and rapamycin drug treatment [28–30]. In most of these situations, autophagy has both beneficial and harmful effects. It can function as a protective mechanism to promote cell survival in nutritional starvation and other stresses, but excessive autophagy also leads to damage to organelles and even cell death [31,32].

*Aspergillus fumigatus* is an opportunistic filamentous fungus that causes a wide spectrum of life-threatening diseases with poor treatment outcomes in immunocompromised individuals [33]. Calcineurin is considered a potential drug target due to its essential roles in fungal growth and virulence [34–36]. In this study, we observed the phenomenon that exogenous calcium is toxic to calcineurin-mutant fungi. By monitoring the calcium dynamics in the cytosol and intracellular calcium stores with modified forms of aequorin as a calcium reporter, we found that the calcineurin mutant exhibited abnormal calcium homeostasis and triggered autophagy and global fragmentation of the nucleus and organelles under a calcium stimulus. Additionally, the defective phenotypes of the calcineurin mutant can be significantly suppressed by alleviating cytosolic calcium

overload through deletion of the  $\text{Ca}^{2+}$  channel *cchA* or by increasing vacuolar calcium storage capacity with overexpressed vacuolar P-type  $\text{Ca}^{2+}$ -ATPase PmcA, highlighting the feedback relationship between calcineurin and CchA and the critical role of vacuoles in the detoxification of excess calcium for fungal survival. Our findings shed light on the underlying mechanism by which calcineurin regulates calcium homeostasis for cell survival, and these results provide a rationale for combination therapy of calcium and calcineurin inhibitors to combat human fungal pathogens.

## Results

### Extracellular calcium is toxic to *A. fumigatus* calcineurin mutants

Calcineurin is a highly conserved  $\text{Ca}^{2+}$ -calmodulin-dependent protein phosphatase that plays a central role in morphological development and cation homeostasis in fungi [37,38]. To further characterize the functions of calcineurin in  $\text{Ca}^{2+}$  signaling transduction, we constructed deletion mutants of the catalytic subunit CnaA and the regulatory subunit CnaB by CRISPR-Cas9 technique in *A. fumigatus* (Figure S1). Morphological analysis in solid and liquid minimal media showed that the  $\Delta\text{cnaA}$  mutant displayed defective morphological phenotypes including reduced hyphal growth and abnormal branching (Figure 1a). Notably, the abnormal hyphal phenotypes of the  $\Delta\text{cnaA}$  mutant were exacerbated in the presence of 10 mM  $\text{CaCl}_2$ , i.e., swollen hyphae tips, whereas no obvious differences were observed in the *cnaA<sup>R</sup>* complementary strain. Moreover, the  $\Delta\text{cnaA}$  mutant showed a significant decrease in mycelial production compared to that of the wild-type at indicated time-points when cultured in media with or without 10 mM  $\text{CaCl}_2$  (Figure 1b). Interestingly, the calcineurin mutants ceased growth when incubated in the presence of calcium after 72 h, suggesting that the addition of calcium is toxic to the  $\Delta\text{cnaA}$  mutant (Figure 1c). To confirm this toxicity, we cultured the wild-type and  $\Delta\text{cnaA}$  strains in liquid minimal media (MM) with or without 10 mM  $\text{CaCl}_2$  for 96 h. Subsequently, the homogenized mycelia were inoculated into fresh liquid MM for another 48 h. The wild-type strains pretreated with or without calcium grew relatively well after transferring to fresh liquid MM. In contrast, the growth of the  $\Delta\text{cnaA}$  mutant pretreated with calcium was dramatically decreased compared to that of the untreated  $\Delta\text{cnaA}$  mutant (Figure 1d and e), confirming that the relatively low levels of extracellular calcium significantly inhibited the growth of the calcineurin mutant.

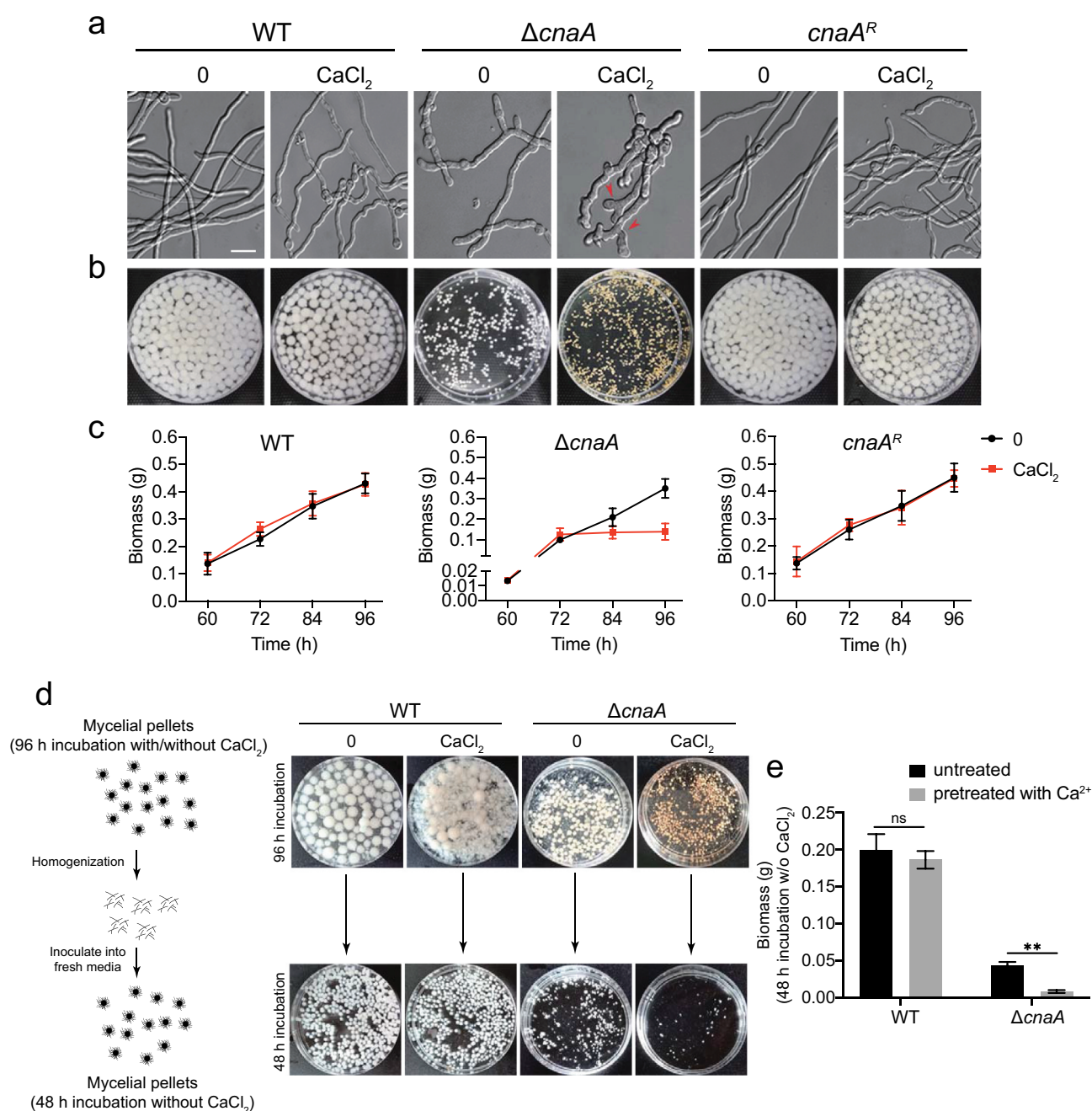


**Figure 1.** Calcium is toxic to calcineurin mutants.

**A.** Differential interference contrast (DIC) images of hyphae grown in liquid MM with or without 10 mM CaCl<sub>2</sub> at 37°C in stationary culture for 14 h. Scale bar represents 10 μm. **B.** The morphology of mycelial pellets of the indicated strains grown in MM with or without 10 mM CaCl<sub>2</sub> at 37°C for 60 h. **C.** Quantification of biomass production for the wild-type,  $\Delta cnaA$ , and  $cnaA^R$  complementary strains grown in MM with or without 10 mM CaCl<sub>2</sub> at different time points (60, 72, 84, and 96 h). **D.** Schematic diagram for determination of calcium toxicity to *A. fumigatus* cells. The wild-type and  $\Delta cnaA$  strains were cultured in liquid MM with or without 10 mM CaCl<sub>2</sub> at 37°C for 96 h. Then, the harvested mycelia were homogenized and inoculated into fresh liquid MM for another 48 h at 37°C. **E.** Quantification of biomass production for the wild-type and  $\Delta cnaA$  strains pretreated with or without 10 mM CaCl<sub>2</sub> grown in liquid MM at 37°C for 48 h. Statistical significance was determined by Student's *t*-test. \*\**p* < 0.01.

Moreover, the  $\Delta cnaB$  mutant exhibited identical phenotypes to those of the  $\Delta cnaA$  mutant under the conditions we tested (Figure S2). Taken together, these data suggest that extracellular calcium is toxic to

*A. fumigatus* calcineurin mutants and that calcineurin is essential for the survival of *A. fumigatus* in response to calcium stimuli. Given that  $\Delta cnaB$  displayed the identical phenotype to the  $\Delta cnaA$  mutant in the

presence of calcium and previous study showed that both of catalytic subunit CnaA and regulatory subunit CnaB are indispensable for the function of calcineurin [39], we therefore chose the  $\Delta cnaA$  mutant for subsequent experiment to investigate the role of calcineurin in mediating the cellular physiology process.

### ***$\Delta cnaA$ mutant exhibits increased cytosolic and vacuolar calcium accumulation in response to extracellular calcium stimuli***

Given that calcineurin is critical for regulating *A. fumigatus* survival in response to extracellular calcium, to further explore the mechanisms by which calcineurin regulates calcium homeostasis in *A. fumigatus*, we constructed wild-type and calcineurin mutants expressing codon-optimized aequorin to perform real-time monitoring of the dynamics of free  $\text{Ca}^{2+}$  concentration  $[\text{Ca}^{2+}]_c$  in living hyphal cells [40]. Upon treatment with 10 mM  $\text{CaCl}_2$ , the  $[\text{Ca}^{2+}]_c$  (the free  $\text{Ca}^{2+}$  concentration in cytosol) in the wild-type strain transiently increased from a basal resting level of approximately 0.1  $\mu\text{M}$  to a peak concentration of 0.63  $\mu\text{M}$  and then gradually returned to a stable resting level (Figure 2a); thus, the amplitude of  $[\text{Ca}^{2+}]_c$  between the peak and the resting status was 0.55  $\mu\text{M}$ . In comparison, the basal resting level of  $[\text{Ca}^{2+}]_c$  increased from 0.1  $\mu\text{M}$  to 0.2  $\mu\text{M}$  (~2-fold increase) and amplitude of  $[\text{Ca}^{2+}]_c$  increased from 0.55  $\mu\text{M}$  to 0.73  $\mu\text{M}$  (~33% increase) in the  $\Delta cnaA$  mutant under the same conditions, suggesting that cytosolic calcium homeostasis was affected by the deletion of *cnaA*. Next, we wondered whether the calcium equilibrium in mitochondria would be affected by calcineurin mutants. To test this possibility, we compared the  $[\text{Ca}^{2+}]_{\text{mt}}$  (the free  $\text{Ca}^{2+}$  concentration in mitochondria) using a modified aequorin (Mt-Aeq) protein fused with a mitochondrial signal peptide. As shown in Figure 2b, the  $\Delta cnaA$  mutant displayed a 20% increase in the basal resting level and a similar amplitude response of  $[\text{Ca}^{2+}]_{\text{mt}}$  compared to the wild-type and *cnaA* complementing strains, suggesting that the deletion of *cnaA* only has a minor effect on mitochondrial calcium homeostasis. Next, we wondered in fungi, the vacuole might be a major intracellular  $\text{Ca}^{2+}$  store that plays a role in the regulation of  $\text{Ca}^{2+}$  homeostasis. However, until now, no reliable detection approach has been available for the real-time monitoring of the vacuolar-free  $\text{Ca}^{2+}$  concentration ( $[\text{Ca}^{2+}]_{\text{vac}}$ ) in fungi. To set up this system, we fused a guide sequence encoding the vacuolar lumen marker protein carboxypeptidase Y (CpyA) at the N-terminus of aequorin to generate the fusion protein CpyA-Aeq [41]. To verify the localization of the guided protein CpyA in

*A. fumigatus*, we tagged CpyA with GFP and RFP at the C-terminus under control of *gpdA* promoter, respectively. As shown in Figure 2c, the localization of CpyA-GFP fusion protein shows a vacuolar pattern. To further verify this localization, we tagged the previously reported vacuole membrane-localized protein PmcA (the homolog of yeast P-type  $\text{Ca}^{2+}$ -ATPase Pmc1) with GFP in the CpyA-RFP background. Colocalization analysis showed that GFP-PmcA surrounded the CpyA-RFP (Figure 2c), demonstrating that CpyA acts as a typical vacuole lumen protein. Next, to further confirm the feasibility of the  $[\text{Ca}^{2+}]_{\text{vac}}$  measurement system, we generated the overexpression strains of the vacuolar P-ATPases PmcA and PmcB, which are responsible for calcium influx into the vacuole by consuming ATP, and assessed the calcium levels in the vacuole. As shown in Figure S3, overexpressing *pmcA/B* remarkably elevated the basal resting level of  $[\text{Ca}^{2+}]_{\text{vac}}$  and enhanced calcium influx into the vacuole compared with the wild-type strain, confirming the reliability of this vacuolar calcium measurement method. Thus, we employed the CpyA-Aeq system to monitor the free  $\text{Ca}^{2+}$  concentration of vacuoles. Interestingly, the basal resting  $[\text{Ca}^{2+}]_{\text{vac}}$  level in vacuoles (0.65  $\mu\text{M}$ ) prior to stimuli was significantly greater than that in the cytosol and mitochondria (Figure 2d), confirming that the vacuole is a major intracellular calcium store in *A. fumigatus*. Notably, in the  $\Delta cnaA$  cells, the basal resting level of  $[\text{Ca}^{2+}]_{\text{vac}}$  was 0.8  $\mu\text{M}$  (~23% increase) and the  $[\text{Ca}^{2+}]_{\text{vac}}$  amplitude was 4.6  $\mu\text{M}$  (~5-fold increase) compared to that of in wild-type cells upon exposure to 10 mM  $\text{Ca}^{2+}$  (Figure 2d). Collectively, these data suggested that the  $\Delta cnaA$  mutant exhibits a dramatic increase in vacuolar  $\text{Ca}^{2+}$  influxes and induces excessive vacuolar  $\text{Ca}^{2+}$  accumulation.

### ***Extracellular calcium induces vacuolar fragmentation and autophagy in the $\Delta cnaA$ mutant***

Next, we wondered whether the excessive vacuolar  $\text{Ca}^{2+}$  accumulation in the  $\Delta cnaA$  mutant would cause any changes of vacuolar morphology. As shown in Figure 3a, fluorescence microscopy analysis showed that wild-type and  $\Delta cnaA$  cells had similar oval-shaped mature vacuoles as indicated by CpyA-GFP when cultured in liquid minimal media for 36 h with or without the addition of calcium. Notably, when incubation time was prolonged to 60 h, the  $\Delta cnaA$  mutant showed highly fragmented fluorescence patterns of vacuoles in the presence of calcium (Figure 3a), even at a calcium concentration as low as 0.1 mM (Figure S4A), suggesting that the addition of lower concentrations of calcium

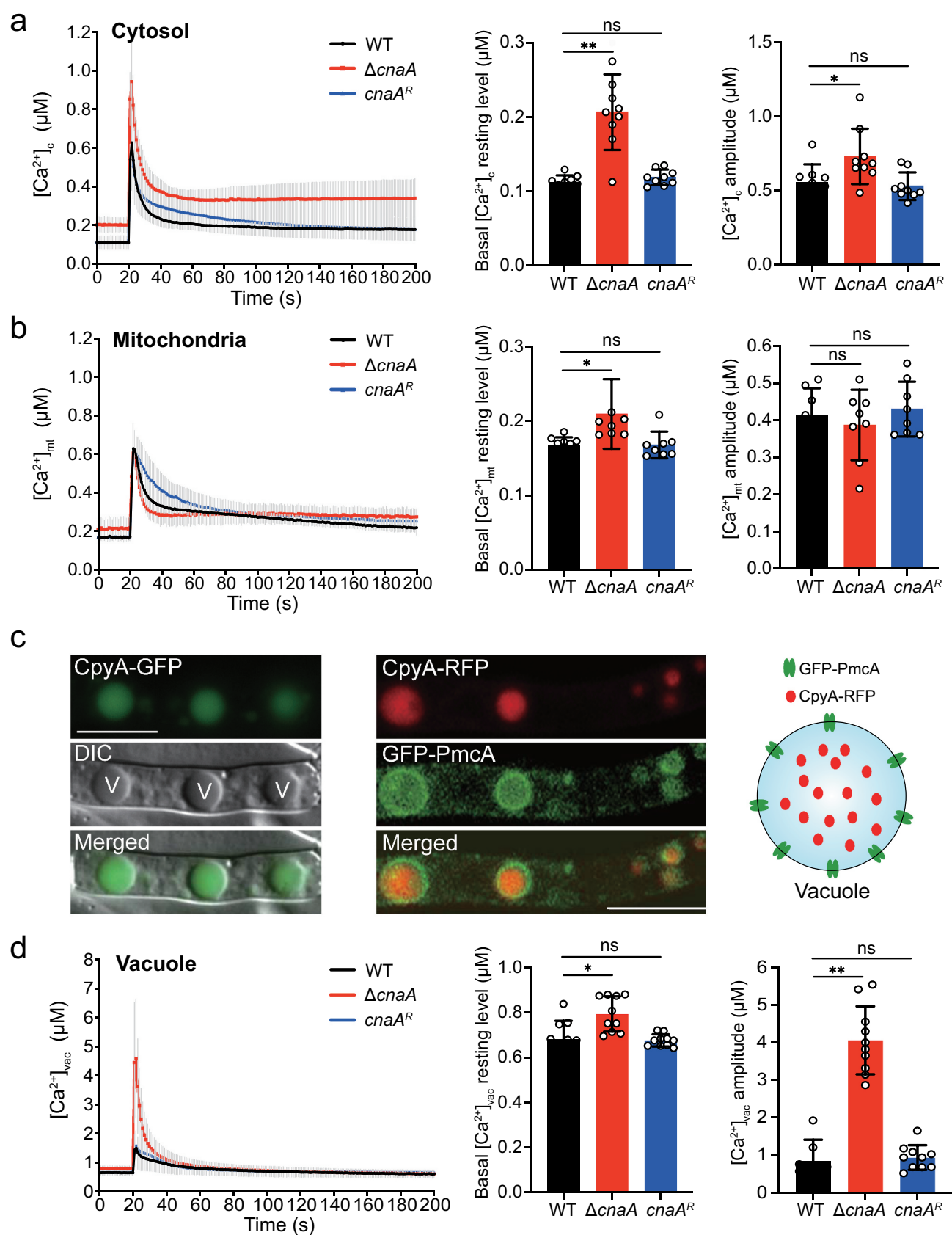


**Figure 2.** Deletion of *cnaA* affects intracellular calcium accumulation in response to extracellular calcium stimuli.

**A, B, and D.** The linear graphs indicate the real-time  $[Ca^{2+}]_c$ ,  $[Ca^{2+}]_{mt}$ , and  $[Ca^{2+}]_{vac}$  changes in response to calcium stimuli.  $[Ca^{2+}]_c$ , the free  $Ca^{2+}$  concentration in cytosol;  $[Ca^{2+}]_{mt}$ , the free  $Ca^{2+}$  concentration in mitochondria;  $[Ca^{2+}]_{vac}$ , the free  $Ca^{2+}$  concentration in vacuoles. Basal

$[Ca^{2+}]_c$ , the resting level prior to extracellular calcium stimulus, and  $[Ca^{2+}]_v$  amplitude, the difference between the basal  $[Ca^{2+}]_c$  level and the poststimulatory peak value, are presented. Data are the average of at least six experiments. Error bars show the standard deviation. Statistical significance was determined by Student's *t*-test. \* $p < 0.05$ ; \*\* $p < 0.01$ ; ns, not significant. **C.** The localization of CpyA. The letter V in the DIC image indicates vacuole (Left). The localization analysis (Middle) and schematic illustration (Right) of PmcA and CpyA. Scale bar represents 5  $\mu$ m.

may result in calcium toxicity in the  $\Delta cnaA$  mutant under *in vitro* laboratory condition. In comparison, in the absence of calcium treatment, the vacuolar morphologies of  $\Delta cnaA$  mutants showed no detectable differences compared to the parental strain. These data indicate that significant vacuolar fragmentation occurs in the  $\Delta cnaA$  mutant when grown in liquid minimal media containing extra calcium. Because the vacuole is the major site for macromolecular degradation through autophagy, to examine whether the deletion of *cnaA* would trigger autophagy under extracellular calcium condition, we generated double-labeled strains with the autophagy marker Atg8 tagged at its N-terminus with GFP and the vacuole marker CpyA fused with RFP and monitored these in the  $\Delta cnaA$  and wild-type backgrounds. As shown in Figure 3b, GFP-Atg8 fusion proteins show a punctate pattern that is proximal to the CpyA-RFP-labeled vacuoles in the wild-type and  $\Delta cnaA$  strains when incubated for 36 h in the presence or absence of calcium. However, when cultures were stimulated by the addition of  $CaCl_2$  for 60 h, the green fluorescence patterns of GFP-Atg8 overlapped with the CpyA-RFP-labeled vacuoles (Figure 3b). Furthermore, Western blotting showed that the  $\Delta cnaA$  strain displayed increased cleavage of GFP from the GFP-Atg8 fusion protein compared to the wild-type cells when cultured for 60 h under the control of the constitutive *gpdA* promoter (Figure 3c) or the native *atg8* promoter (Figure S4B-S4C) in the presence of calcium. In addition, cleavage of GFP was not significantly exacerbated when media were supplemented with other divalent metal cations including magnesium, zinc, iron, and copper (Figure S4D), suggesting that the autophagy was specifically induced by calcium. Next, to examine the contribution of autophagy to  $Ca^{2+}$  toxicity in the  $\Delta cnaA$  mutant, we deleted the classic autophagy-dependent gene *atg2*, which encodes a peripheral membrane protein for autophagic vesicle formation [42,43], in the  $\Delta cnaA$  background. As shown in Figure 3d, GFP-Atg8 consistently exhibited a punctate pattern and did not co-localize with the vacuolar marker CpyA-RFP in the  $\Delta cnaA\Delta atg2$  mutant. Furthermore, Western blotting showed that no (or an undetectable level of) GFP was cleaved from GFP-Atg8 fusion protein in the  $\Delta cnaA\Delta atg2$  double mutant compared with the  $\Delta cnaA$  mutant (Figure 3e), suggesting that autophagy was suppressed in the  $\Delta cnaA\Delta atg2$  mutant.

Notably, as shown in figure 3f, the  $\Delta cnaA\Delta atg2$  mutant displayed a delay in growth cessation (at 84 h) compared to that of the  $\Delta cnaA$  mutant (at 72 h) under calcium treatment conditions (figure 3f). However, the  $\Delta cnaA\Delta atg2$  mutant pretreated with or without calcium showed a comparable biomass production compared to that of the  $\Delta cnaA$  mutant after homogenization and transfer to fresh liquid MM, suggesting that the deletion of *atg2* did not prevent the cell death induced by a lack of *cnaA* after culture (Figure 3g), indicating that Atg2 is required for autophagy but not  $Ca^{2+}$  toxicity in the calcineurin-deficient mutant upon calcium stimuli. Taken together, these data suggest that a lack of CnaA results in specific calcium-induced autophagy in *A. fumigatus*.

#### **Lack of the calcium channel CchA alleviates the calcium toxicity-related phenotypes in the *cnaA* null mutant**

Our previous studies in a model fungus *A. nidulans* indicated that calcineurin negatively regulates CchA (the voltage-gated  $Ca^{2+}$  channel component of high-affinity calcium influx system) upon calcium uptake in response to extracellular calcium; the deletion of *cchA* suppressed the hypersensitivity to external calcium in calcineurin mutants [44]. We hypothesized that a similar situation would occur in *A. fumigatus*. As expected, *cchA* deletion partially suppressed the colony radial growth defects and hyperbranching polarity growths in *cnaA* deletion mutants with or without calcium treatment (Figure S5). Notably, a lack of CchA significantly rescued the defective hyphal growth of the *cnaA* mutant in calcium treatment conditions (Figure 4a and b). The detection of calcium dynamics in living cells showed that the  $[Ca^{2+}]_{vac}$  amplitude and the basal resting  $[Ca^{2+}]_c$  of the  $\Delta cnaA\Delta cchA$  mutant were approximately 53% and 20% lower, respectively, than those in the  $\Delta cnaA$  mutant (Figure 4c and d), suggesting that calcineurin mediates cytosolic and vacuolar calcium homeostasis by negatively regulating CchA. Accordingly, the colocalization of GFP-Atg8 and CpyA-RFP (vacuolar marker) and the vacuolar fragmentation were not observed in the  $\Delta cnaA\Delta cchA$  mutant (Figure 4e). Moreover, Western blots showed that the  $\Delta cnaA\Delta cchA$  mutant exhibited an autophagy

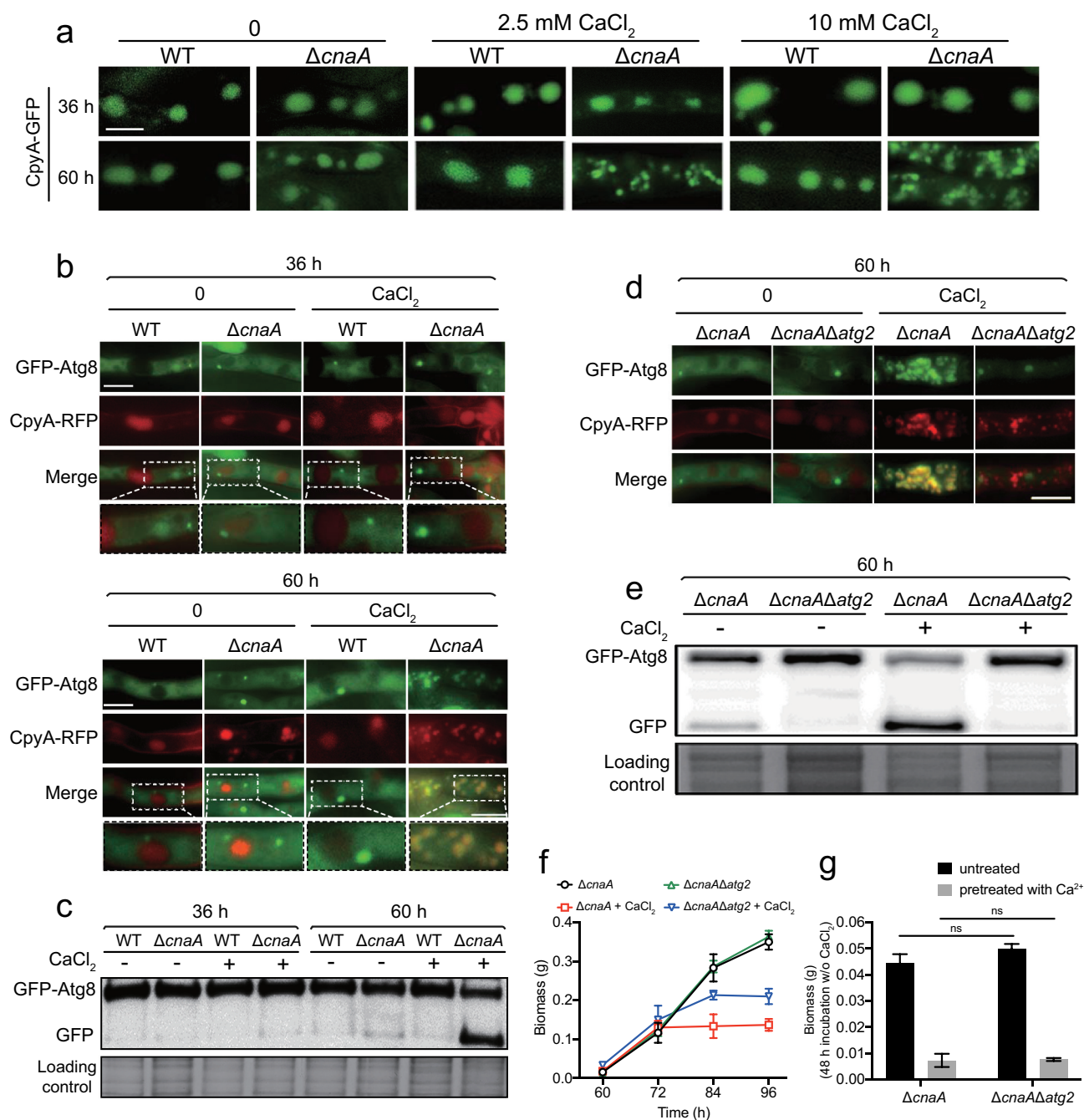


**Figure 3.** The loss of CnaA causes vacuolar fragmentation and *atg2*-related autophagy in the presence of excess calcium.

**A.** Vacuolar morphology was monitored by fluorescence microscopy using CpyA-GFP as vacuolar lumen marker. The indicated strains were grown in liquid MM with or without CaCl<sub>2</sub> for 36 and 60 h. Scale bar represents 5 μm. **B and D.** The localization of CpyA-RFP and GFP-Atg8 was used to monitor the autophagy process. When autophagy is induced, the outer membrane of the autophagosome was fused with the membrane vacuole, whereas the inner membranes and the cargo were delivered into the vacuolar lumen for degradation. In this process, the Atg8 protein transferred from the autophagosome to the vacuole and was cleaved. The GFP/RFP signals in the mycelium pellets were observed after the indicated strains were cultured in a rotary shaker with or without 10 mM CaCl<sub>2</sub> for 36 or 60 h. Scale bars represent 5 μm. **C and E.** Western blotting showed the GFP-Atg8 cleavage of the related strains in MM with or without 10 mM CaCl<sub>2</sub> for 36 or 60 h. The extent of autophagy was estimated by calculating the amount of free GFP compared to the total amount of GFP-Atg8 and free GFP. Coomassie blue staining served as a loading control. **F.** Quantification of biomass production for the ΔcnaA and ΔcnaAΔatg2 strains grown in MM with or without 10 mM CaCl<sub>2</sub> at different time points (60, 72, 84, and 96 h). **G.** Quantification of biomass production for the ΔcnaA and ΔcnaAΔatg2 strains pretreated with or without 10 mM CaCl<sub>2</sub> grown in liquid MM at 37°C for 48 h. Statistical significance was determined by Student's *t*-test. ns, not significant.

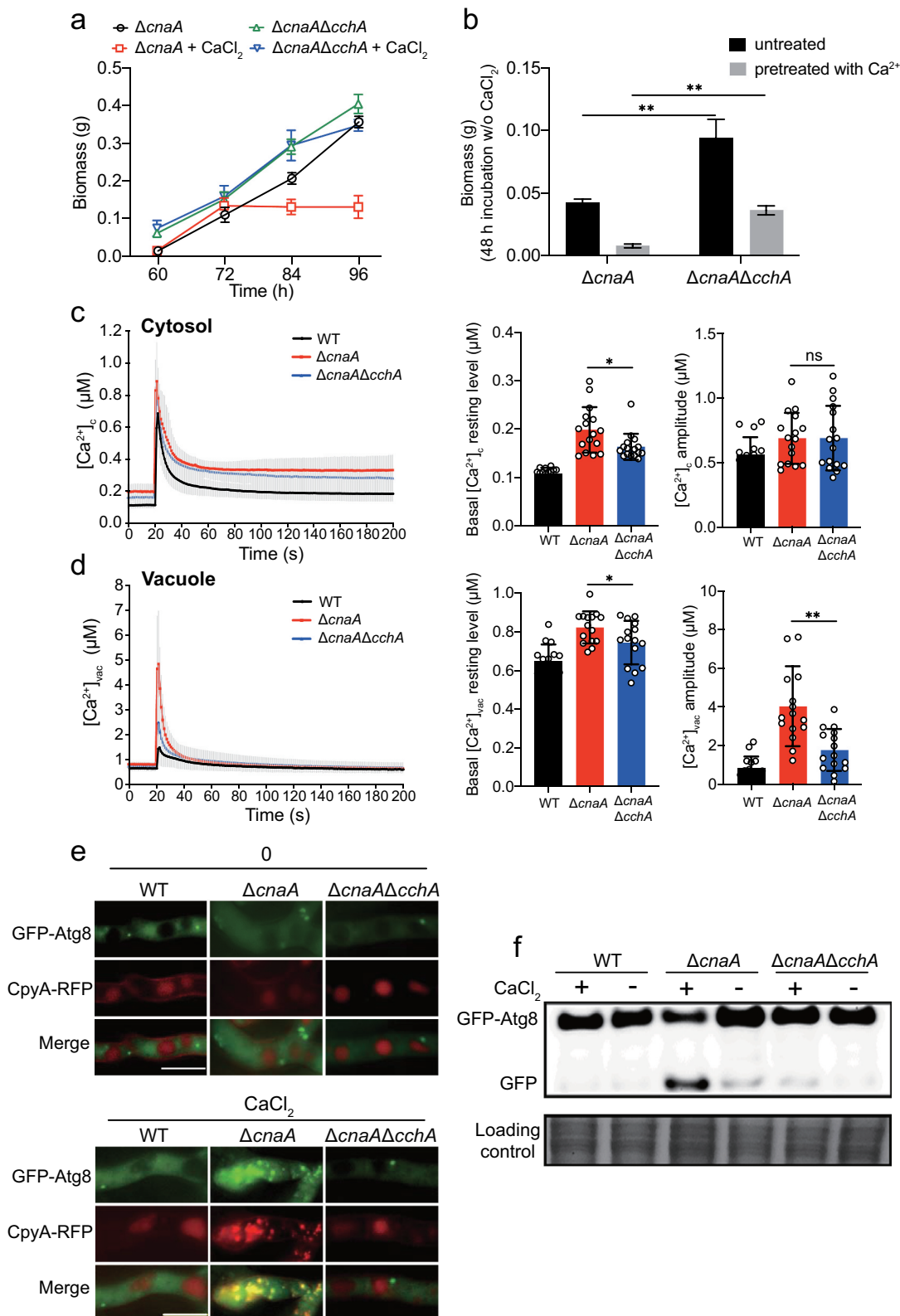


**Figure 4.** Deletion of *cchA* alleviates the calcium toxicity-related phenotypes in the  $\Delta cnaA$  mutant.

**A.** Quantification of biomass production for the  $\Delta cnaA$  and  $\Delta cnaA\Delta cchA$  strains grown in MM with or without 10 mM  $CaCl_2$  at different time points (60, 72, 84 and 96 h). **B.** Quantification of biomass production for the  $\Delta cnaA$  and  $\Delta cnaA\Delta cchA$  strains pretreated with or without 10 mM  $CaCl_2$  grown in liquid MM at 37°C for 48 h. Statistical significance was determined by Student's *t*-test.  $**p < 0.01$ . **C and D.** The comparison of  $[Ca^{2+}]_c$  and  $[Ca^{2+}]_{vac}$  of WT,  $\Delta cnaA$  and  $\Delta cnaA\Delta cchA$  in resting and dynamic level.  $*p < 0.05$ ;  $**p < 0.01$ ; ns, not significant. **E and F.** The co-localization analysis of CpyA-RFP and GFP-Atg8 and Western blotting showed the localization and cleavage of GFP-Atg8 of the related strains in MM with or without 10 mM  $CaCl_2$  for 60 h. Scale bars represent 5  $\mu m$ .



level similar to that of the wild-type strain (figure 4f), suggesting that autophagy in response to external calcium is inhibited when *cchA* is deleted in the  $\Delta cnaA$  mutant. These data suggest that a lack of the calcium channel CchA alleviates the calcium toxicity-related phenotypes in the *cnaA* null mutant.

### Lack of CchA did not restore the virulence of the $\Delta cnaA$ mutant in a mouse infection model

The aforementioned data demonstrated that the absence of CchA in the  $\Delta cnaA$  mutant partially suppressed the growth defects of *A. fumigatus* *in vitro*. Next, we further tested whether the  $\Delta cnaA\Delta cchA$

mutant would affect virulence in *in vivo* animal models. As shown in Figure 5, immunocompromised ICR mice were infected with fresh conidia, homogenized hyphae, or luciferase-probed related strains by an intratracheal route. After two weeks, the mice infected with wild-type *A. fumigatus* display high mortality, whereas both the  $\Delta cnaA\Delta cchA$  and  $\Delta cnaA$  mutants caused low mortality (Figure 5a). Statistical analysis showed that there was no significant difference between  $\Delta cnaA\Delta cchA$  and  $\Delta cnaA$  in survival rates for either the conidia or the homogenized hyphal infection model. Histopathological examinations and live animal imaging showed that the lungs from mice inoculated with the wild-type fungus displayed aggressive fungal growth

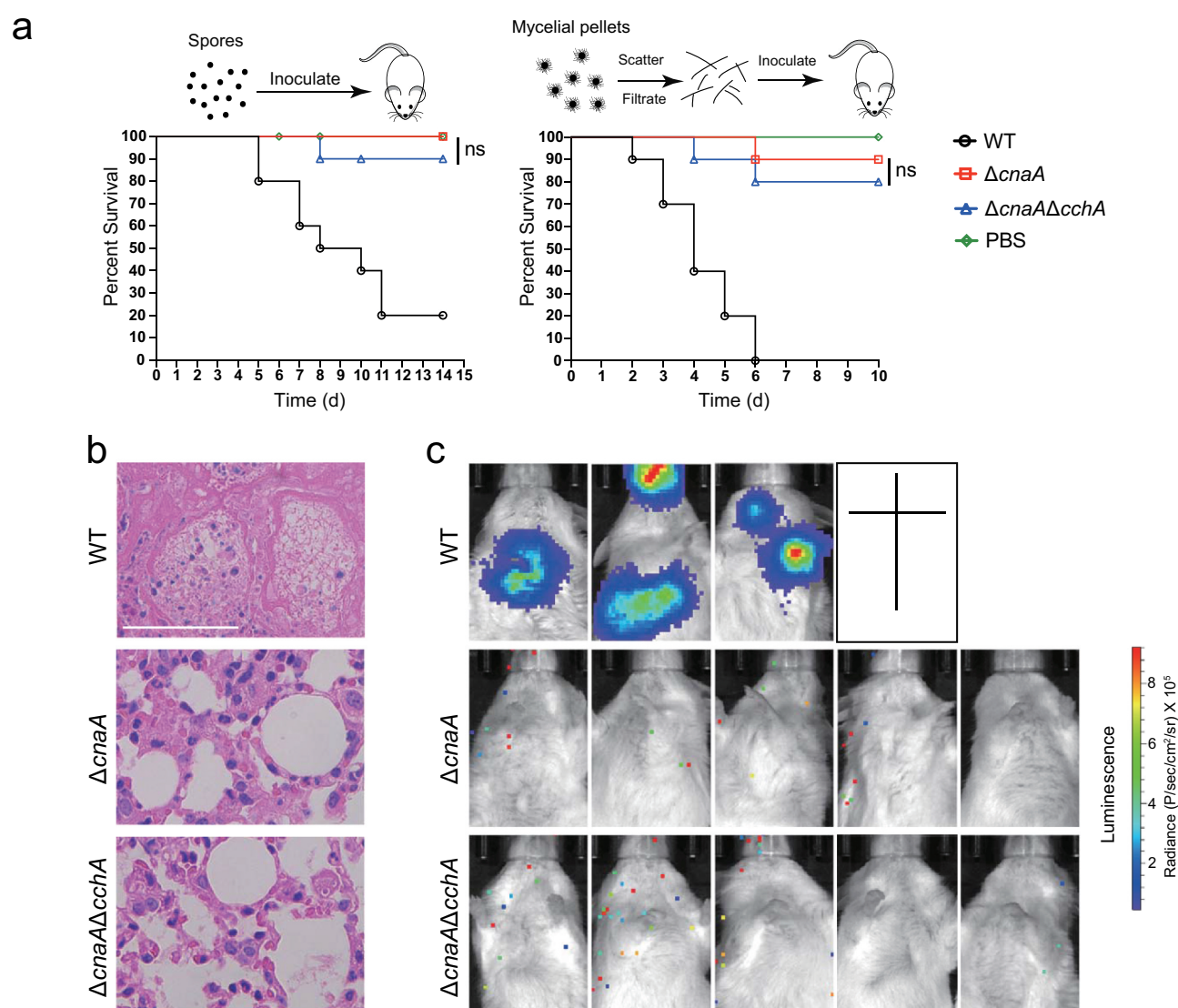


**Figure 5.** Deletion of *cchA* in the  $\Delta cnaA$  mutant did not restore the virulence in a mouse infection model.

**A.** Survival curve of mice infected with conidia or hyphae (middle and right panels) of WT,  $\Delta cnaA$ , and  $\Delta cnaA\Delta cchA$  *A. fumigatus*. Statistical analysis between groups was done using the log-rank test. ns, not significant. **B.** Histopathological sections of lung tissue from sacrificed mice infected with conidia of each strain. Periodic acid-Schiff stain was used to visualize fungal growth. Scale bar represents 50  $\mu$ m. **C.** Luciferase signals in mice infected with hyphae were measured with a live animal imaging system 4 days after infection.

and luminescence signals around the lungs (Figure 5b and c). In contrast, there was no detectable fungal growth or luminescence signals in the lungs of mice infected with the  $\Delta cnaA\Delta cchA$  or  $\Delta cnaA$  mutants, the differences in virulence are likely due to the different immune systems between these two infection models. Together, these data suggest that the lack of CnaA results in the loss of virulence in immunocompromised mice, and the deletion of *cchA* did not restore the virulence in the mouse model.

### Overexpressing P-type $\text{Ca}^{2+}$ -ATPase PmcA significantly rescued the calcium toxicity-related phenotypes in the $\Delta cnaA$ mutant

In fungi, the vacuole serves as the major  $\text{Ca}^{2+}$  store and plays a critical role in the detoxification of cytoplasmic  $\text{Ca}^{2+}$ . Vacuolar calcium equilibrium is maintained by the P-type  $\text{Ca}^{2+}$ -ATPase Pmc family and the  $\text{H}^+/\text{Ca}^{2+}$  exchanger Vcx family, which are regulated by calcineurin [4]. In line with this information, the  $\Delta cnaA$  mutant exhibited lower expression levels of *pmcA* and *pmcC* compared to those of the wild-type, whereas the transcript level of vacuolar  $\text{H}^+/\text{Ca}^{2+}$  exchanger family members, especially *vcxB*, *vcxD*, and *vcxE*, was upregulated in *A. fumigatus* (Figure S6), demonstrating that calcineurin positively regulates the P-type  $\text{Ca}^{2+}$ -ATPase Pmc family while negatively regulating the  $\text{H}^+/\text{Ca}^{2+}$  exchanger Vcx family. Given the calcium toxicity-related phenotypes observed in the  $\Delta cnaA$  mutant, we hypothesized that the upregulation of  $\text{H}^+/\text{Ca}^{2+}$  exchanger Vcx family members in the  $\Delta cnaA$  mutant would be insufficient to detoxify excess cytoplasmic calcium in response to external calcium, and thus a  $\Delta cnaA^{OE::pmcA}$  strain overexpressing PmcA, the yeast P-type  $\text{Ca}^{2+}$ -ATPase Pmc1 homolog in *A. fumigatus*, under the control of the strong constitutive promoter  $P_{\text{gpdA}}$  was used in the  $\Delta cnaA$  background to test whether the defective phenotypes in the  $\Delta cnaA$  mutant would be suppressed. qRT-PCR analysis confirmed that *pmcA* was highly overexpressed in the  $\Delta cnaA$  mutant (Figure S3). Further live-cell detection of  $[\text{Ca}^{2+}]_{\text{vac}}$  showed that the  $\Delta cnaA^{OE::pmcA}$  strain displayed an elevated basal resting level of  $[\text{Ca}^{2+}]_{\text{vac}}$  and had an enhanced  $[\text{Ca}^{2+}]_{\text{vac}}$  amplitude compared to that of the  $\Delta cnaA$  mutant (Figure 6a), indicating that calcium was effectively transported from the cytoplasm to vacuoles by PmcA. Additionally, autophagy assays showed that the  $\Delta cnaA^{OE::pmcA}$  strain displayed reduced autophagy compared to that of the  $\Delta cnaA$  mutant in response to external calcium stimuli (Figure 6b and c). Moreover, the overexpression of *pmcA* in the *cnaA* mutant markedly suppressed the growth cessation in calcium

treatment conditions (Figure 6d). The  $\Delta cnaA^{OE::pmcA}$  strain pretreated with or without calcium (96 h) showed dramatically increased biomass production compared to that of the  $\Delta cnaA$  mutant after homogenization and transfer to fresh liquid MM (Figure 6e). Thus, these data suggested that overexpressing P-type  $\text{Ca}^{2+}$ -ATPase PmcA partially rescues calcium toxicity-related phenotypes in the  $\Delta cnaA$  mutant.

### The $\Delta cnaA$ mutant exhibits global fragmentation of nuclei and organelles upon calcium stimuli

To further dissect the molecular mechanisms operating in the *A. fumigatus*  $\Delta cnaA$  mutant upon *in vitro* calcium stimuli, we performed proteomic comparison analysis using tandem mass tags (TMTs) and liquid chromatography tandem MS (LC/MS-MS) and compared wild-type and  $\Delta cnaA$  strains grown in the presence of extracellular calcium for 60 h. Proteins with change ratios significantly different from general protein variation ( $1.50 < \Delta cnaA/\text{wild-type} < 0.50$ ) were selected for gene ontology (GO) annotation and enrichment analysis. As shown in Table S3, the expression levels of 618 and 218 proteins were increased and decreased, respectively, in the  $\Delta cnaA$  mutant compared to the wild-type strain. Most increased abundance of proteins were involved in metabolic processes of biomolecules, especially in catabolism and proteolysis (Figure S7A). In contrast, most of proteins with decreased abundance were associated with biosynthesis and/or the transport of biomolecules and inorganic ions (Figure S7B). Kyoto Encyclopedia of Genes and Genomes (KEGG) annotation revealed that the proteins with increased abundance were primarily associated with various amino acid metabolism pathways, especially tyrosine, beta-alanine, valine, and leucine (Figure 7a), whereas proteins with decreased abundance mainly focused on biosynthesis-related pathways including ribosome (protein synthesis), thiamine metabolism, and steroid biosynthesis. Of note, proteins with increased abundance in the  $\Delta cnaA$  mutant included 23 peptidases, 18 hydrolases, 4 nucleases, 3 proteases, 3 autophagy-related proteins, and 1 metacaspase (Figure 7b), which may lead to global protein degradation and cause apoptosis/apoptotic-like programmed and/or autophagic cell death in  $\Delta cnaA$  cells under calcium treatment. Thus, we hypothesized that CnaA-involved cellular calcium equilibrium may regulate whole-cell organelle networks. To further assess whether a lack of CnaA would induce abnormal organelle and nuclear morphology with calcium treatment, we probed the nucleus (RFP-H2A), endoplasmic reticulum (Erg11A-GFP), Golgi apparatus (RFP-PH<sup>OSBP</sup>), and

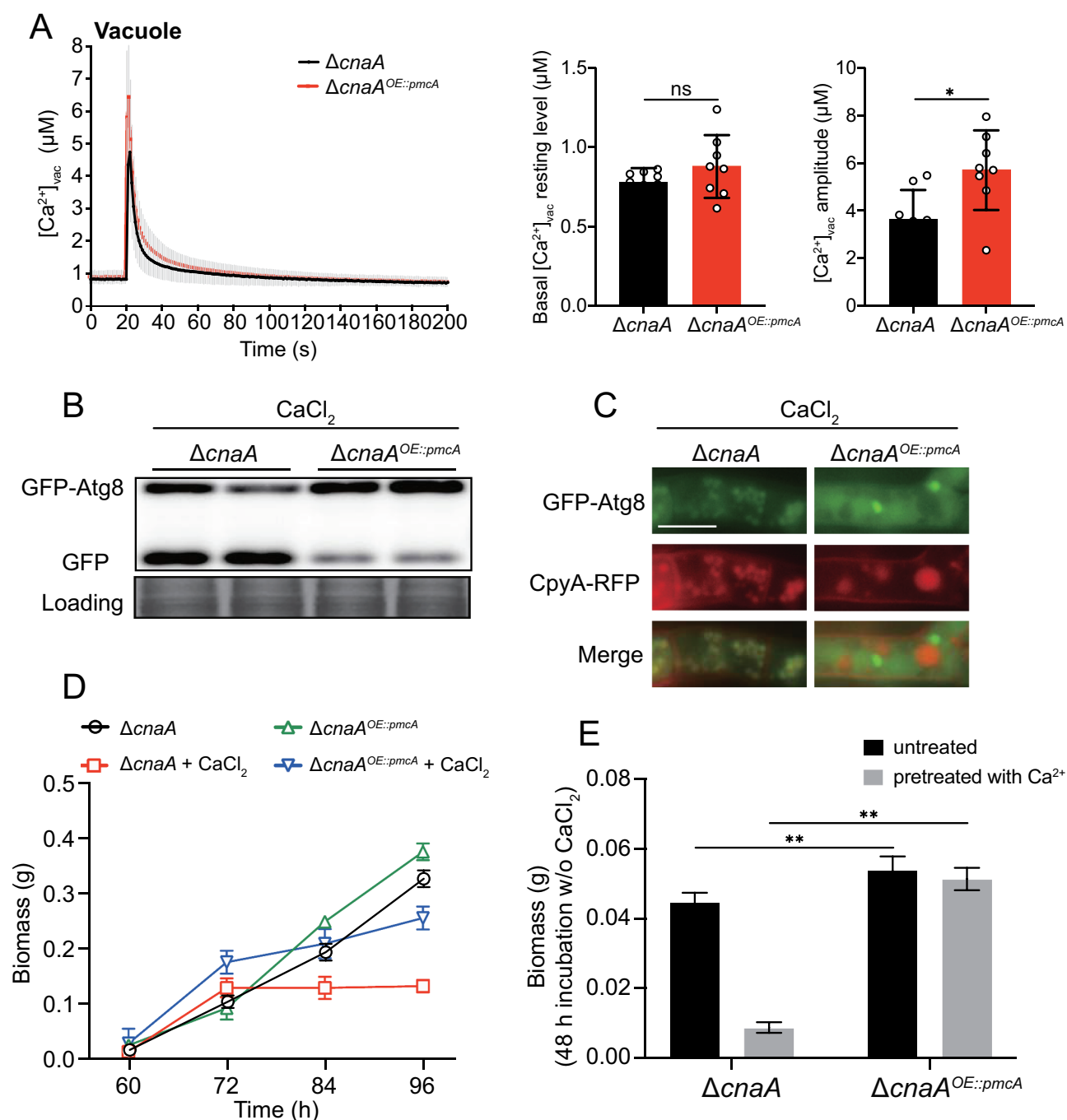


**Figure 6.** Overexpressing P-type Ca<sup>2+</sup>-ATPase PmcA in the  $\Delta cnaA$  mutant significantly rescues calcium toxicity-related phenotypes. **A.** The comparison of [Ca<sup>2+</sup>]<sub>vac</sub> of  $\Delta cnaA$  and  $\Delta cnaA^{OE::pmcA}$  in resting and dynamic level. **B and C.** Western blots analysis and co-localization analysis of CpyA-RFP and GFP-Atg8 were used to estimate the autophagy level in  $\Delta cnaA$  and  $\Delta cnaA^{OE::pmcA}$  strains. Scale bar represents 5 μm. **D.** Quantification of biomass production for the  $\Delta cnaA$  and  $\Delta cnaA^{OE::pmcA}$  strains grown in the indicated conditions at different time points (60, 72, 84 and 96 h). **E.** Quantification of biomass production for the  $\Delta cnaA$  and  $\Delta cnaA^{OE::pmcA}$  strains pretreated with or without 10 mM CaCl<sub>2</sub> grown in liquid MM at 37°C for 48 h. Statistical significance was determined by Student's *t*-test. \*\**p* < 0.01.

mitochondria (MrsA-RFP). As predicted, fluorescence observation showed that these organelles displayed fragmentation that was comparable to that of the vacuole in the  $\Delta cnaA$  mutant after calcium treatment for 60 h, suggesting that the apoptosis/apoptotic-like and/or autophagic cell death may occur (Figure 7c).

A similar phenomenon was observed in *A. fumigatus* cells treated with the calcineurin inhibitor FK506 (Figure 7d). The biomass production of the wild-type strain pretreated with FK506 and calcium (96 h) was markedly compared to that of the wild-type strain merely pretreated with FK506 after homogenization

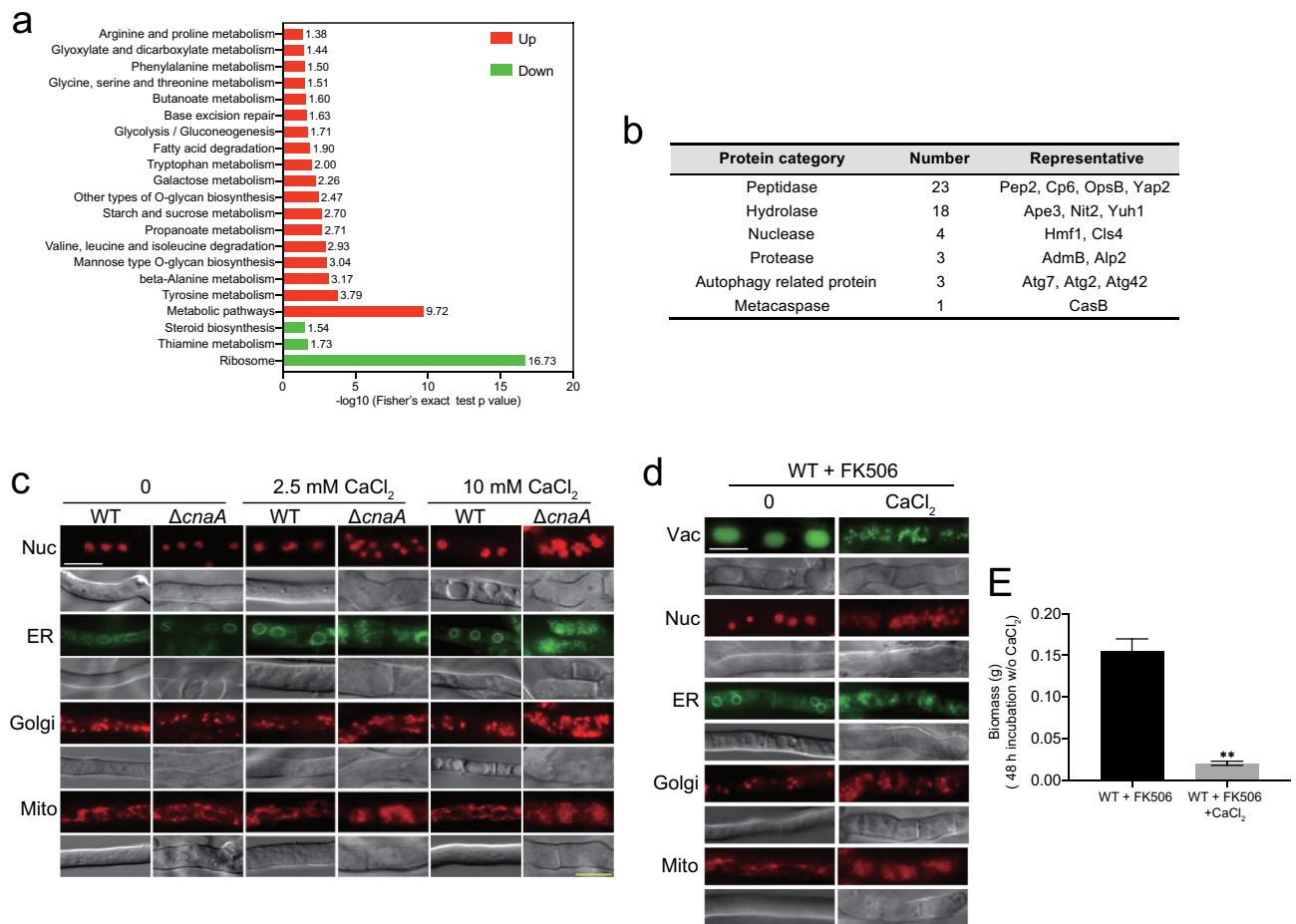


**Figure 7.**  $\Delta cnaA$  mutant shows global fragmentation of nuclei and organelles upon calcium stimuli.

**A.** The indicated strains were grown in MM with 10 mM  $\text{CaCl}_2$  at 37°C for 60 h. KEGG pathways enriched in proteins with more than 1.5-fold changes between WT and  $\Delta cnaA$ . Red and green items indicate increased abundance and decreased abundance pathways, respectively. The KEGG online service tool KAAS ([http://www.genome.jp/kaas-bin/kaas\\_main](http://www.genome.jp/kaas-bin/kaas_main)) was used to annotate protein KEGG database descriptions. **B.** Selected increased abundance of proteins related to material degradation are presented. **C.** The organelle morphologies of the wild-type and  $\Delta cnaA$  strains grown in liquid MM with or without calcium for 60 h. Scale bar represents 5  $\mu\text{m}$ . **D.** The organelle morphologies of the wild-type strain grown in liquid MM supplemented with FK506 in the presence or absence of 2.5 mM  $\text{CaCl}_2$  for 60 h. A 50  $\mu\text{l}$  sample of 2 mM FK506 was added into 100 ml liquid MM at 0 and 48 h during culture. Scale bar represents 5  $\mu\text{m}$ . **E.** Quantification of biomass production for the wild-type strain pretreated with or without 10 mM  $\text{CaCl}_2$  grown in liquid MM supplemented with FK506 at 37°C for 48 h. Statistical significance was determined by Student's *t*-test.  $^{**}p < 0.01$ .

and transfer to fresh liquid MM (Figure 7e). Taken together, these data suggested that global nuclear and organelle fragmentation may contribute to calcium toxicity in mutants lacking functional calcineurin.

## Materials and methods

### Strains, media, and culture conditions

*A. fumigatus* strains used in this study was listed in the supplementary data Table S1. Strains were routinely grown in the following media: minimal media (MM) containing 1% glucose, 2% agar, trace elements and 20  $\times$  salt solution, as described previously [45]. MM supplemented with 5 mM uridine and 10 mM uracil were used for uracil and uridine

auxotroph strains. The recipe for liquid glucose minimal media is identical to that for MM, except without agar. All strains were cultured at 37°C.

### Quantification of biomass production

$10^5$  conidia were incubated in 100 ml of MM with or without 10 mM  $\text{CaCl}_2$  at 37°C in a rotary shaker at 200 rpm for 60, 72, 84, and 96 h. Biomass curves were drawn after mycelial pellets were collected, dried, and weighed.

### Assessment of hyphal survival

The related strains were grown in liquid MM with or without 10 mM  $\text{CaCl}_2$  with 220 rpm shaking at 37°C

for 96 h. Subsequently, the mycelium pellets of each strain were crushed and homogenized into hyphae fragments using tissue grinding and filtered with lens-cleaning paper in sterile ddH<sub>2</sub>O. The optical density at 600 nm (OD<sub>600</sub>) of each group was finally adjusted to 0.2. Then, 100 µl of suspension containing hyphae fragments was inoculated into liquid MM for 48 h via shake cultivation, and the biomass was weighed and compared.

### Constructions for plasmids

For the construction of complementary *cnaA/cnaB*, p-zero-hph-*cnaA* plasmid was generated as follows: the selectable marker *hph* from PAN7-1 was amplified by PCR using the primers *hph*-F and *hph*-R and then cloned into the pEASY-Blunt vector (TransGen Biotech), generating the plasmid p-zero-hph. The primers *cnaA/cnaB*-*notI*-F and *cnaA/cnaB*-*notI*-R were used to generate a fragment that includes the promoter sequence, the complete ORF, and the 3'UTR of *cnaA/cnaB*. This fragment was then cloned into the *NotI* site of p-zero-hph to generate the plasmid p-zero-hph-*cnaA/cnaB*.

For measuring the Ca<sup>2+</sup> level in the cytosol and mitochondria, the plasmids pAMA1-P<sub>gpdA</sub>-Aeq and pAMA1-P<sub>gpdA</sub>-mt-Aeq were generated as follows: PCR was performed using the primers Ama1-BamHI-gpd-F and Ama1-BamHI-trpC-R to amplify P<sub>gpdA</sub>-Aeq-T<sub>trp</sub> and P<sub>gpdA</sub>-mt-Aeq-T<sub>trpC</sub> fragments from the existing plasmids pAEQS1-15 and pAEQ<sub>m</sub> [40,46,47]. The fragments were subcloned into the *BamHI* site of the plasmid prg3-AMAI-NotI to generate pAMA1-P<sub>gpdA</sub>-Aeq and pAMA1-P<sub>gpdA</sub>-mt-Aeq, respectively.

For monitoring the calcium level in the vacuole, the plasmid pAMA1-P<sub>gpdA</sub>-CpyA-Aeq was generated as follows: PCR was performed using the primers ClaI-cpyA-R and ClaI-cpyA-F to generate a *cpyA*' ORF fragment. The fragment was subcloned into the *ClaI* site of pBARGPE, which has a P<sub>gpdA</sub> promoter in front of its *ClaI* site, to generate the plasmid pBARGPE-P<sub>gpdA</sub>-cpyA. The P<sub>gpdA</sub>-cpyA fragment was amplified from the pBARGPE-P<sub>gpdA</sub>-cpyA with Ama1-BamHI-gpd-F and CpyA-linker-R primers and then fused with Aeq-TrpC fragment generated using Linker-Aeq-F and Ama1-BamHI-trpC-R to yield fusion fragment P<sub>gpdA</sub>-cpyA-Aeq. The pAMA1-P<sub>gpdA</sub>-CpyA-Aeq plasmid was generated by ligating P<sub>gpdA</sub>-cpyA-Aeq into prg3-AMAI-NotI.

pAMA1-P<sub>gpdA</sub>-CpyA-GFP/RFP was generated as follows: Fusion PCR using primers Ama1-BamHI-gpd-F and Ama1-BamHI-GFP/RFP-R, was performed to fuse the P<sub>gpdA</sub>-cpyA with GFP/RFP fragment amplified by primers Linker-GFP/RFP-F and Ama1-BamHI-GFP

/RFP-R. Then, the fusion fragment was ligated into the *BamHI* site of the plasmid prg3-AMAI-NotI, generating pAMA1-P<sub>gpdA</sub>-CpyA-GFP/RFP.

For indicating the vacuole, the plasmid pAMA1-P<sub>gpdA</sub>-CpyA-GFP/RFP was generated as follows: Fusion PCR using primers Ama1-BamHI-gpd-F and Ama1-BamHI-GFP/RFP-R, was performed to fuse the P<sub>gpdA</sub>-cpyA with GFP/RFP fragment amplified by primers Linker-GFP/RFP-F and Ama1-BamHI-GFP/RFP-R. Then, the fusion fragment was ligated into the *BamHI* site of the plasmid prg3-AMAI-NotI to generate pAMA1-P<sub>gpdA</sub>-CpyA-GFP/RFP.

For visualization of cell nucleus, the pAMA1-P<sub>gpdA</sub>-RFP-H<sub>2</sub>A was generated as follows: The P<sub>gpdA</sub>-RFP-H<sub>2</sub>A fragment was amplified from the pBARGPE-P<sub>gpdA</sub>-RFP-H<sub>2</sub>A with primers Ama1-BamHI-gpd-F and Ama1-BamHI-trpC-R and then was subcloned into the *BamHI* site of the plasmid prg3-AMAI-NotI to generate pAMA1-P<sub>gpdA</sub>-RFP-H<sub>2</sub>A.

For visualization of ER, the plasmid pAMA1-P<sub>gpdA</sub>-erg11A-GFP was generated as follows: using primers Ama1-BamHI-gpd-F and Erg11A-R, the P<sub>gpdA</sub>-erg11A fragment was amplified from the CX23 [48]. Using primers Erg11A-GFP-F and Ama1-BamHI-GFP-R, the GFP was amplified. Then, P<sub>gpdA</sub>-erg11A and GFP were fused together with primers Ama1-BamHI-gpd-F and Ama1-BamHI-GFP-R. Subsequently, the fusion fragment was subcloned into the *BamHI* site of the plasmid prg3-AMAI-NotI to generate pAMA1-P<sub>gpdA</sub>-erg11A-GFP.

For visualization of mitochondria, the plasmid pAMA1-MrsA-RFP was generated as follows: Using primers Ama1-BamHI-MrsA-F and MrsA-R, the MrsA fragment containing *mrsA* promoter and ORF without stop codon was amplified from the *A. fumigatus* genomic DNA (gDNA). The RFP was amplified with primers MrsA-RFP-F and Ama1-BamHI-RFP-R. Then, MrsA fragment and RFP were fused together with primers Ama1-BamHI-MrsA-F and Ama1-BamHI-RFP-R. Subsequently, the fusion fragment was subcloned into the *BamHI* site of the plasmid prg3-AMAI-NotI to generate pAMA1-MrsA-RFP.

For visualization of Golgi apparatus, pAMA1-P<sub>gpdA</sub>-mRFP-PH<sup>OSBP</sup> was generated as follows: The pleckstrin homology domain of the human oxysterol binding protein (PH<sup>OSBP</sup>) was PCR-amplified with primers gpdA-RFP-F and BamHI-PH<sup>OSBP</sup>-R and then fused with P<sub>gpdA</sub> promoter (PCR-amplified with Ama1-BamHI-gpd-F and Gpd-R) using primers Ama1-BamHI-gpd-F and BamHI-PH<sup>OSBP</sup>-R. The fusion fragment was subcloned into *BamHI* site of the plasmid prg3-AMAI-NotI to pAMA1-P<sub>gpdA</sub>-mRFP-PH<sup>OSBP</sup>.

For measuring the level of autophagy, plasmid pAMA1- $P_{\text{gpdA}}$ -GFP-Atg8 overexpressing GFP-Atg8 was generated as follows: PCR, using the joint primers Ama1-BamHI-gpd-F/Gpd-GFP-F/Atg8-F and Gpd-R/Atg8-GFP-R/Ama1-BamHI-Atg8-R, were performed to generate  $P_{\text{gpdA}}$  promoter/GFP/Atg8(ORF) fragments. Next, the fusion fragments  $P_{\text{gpdA}}$ -GFP-Atg8 were generated by fusion PCR with primers Ama1-BamHI-gpd-F and Ama1-BamHI-Atg8-R. The fusion fragments were subcloned into the *Bam*HI site of the plasmid prg3-AMAI-NotI to generate pAMA1- $P_{\text{gpdA}}$ -GFP-Atg8. The plasmid pAMA1- $P_{\text{atg8}}$ -GFP-Atg8 expressing GFP-Atg8 under *atg8* native promoter was generated as follows: PCR, using the joint primers Ama1-Bam1-atg8(p)-F/Atg8(p)-GFP-F and Atg8-promoter-R/Ama1-BamHI-Atg8-R, was used to generate *atg8* promoter/GFP-Atg8 fragments. Next, the two fragments were fused together with primers with primers Ama1-Bam1-atg8(p)-F and Ama1-BamHI-Atg8-R. The fusion fragment was subcloned into the *Bam*HI site of prg3-AMAI-NotI to generate pAMA1- $P_{\text{atg8}}$ -GFP-Atg8.

For assessing the co-localization of CpyA-RFP and GFP-Atg8, the plasmid pAMA1- $P_{\text{gpdA}}$ -CpyA-RFP- $P_{\text{gpdA}}$ -GFP-Atg8 was generated as follows: The fragment  $P_{\text{gpdA}}$ -CpyA-RFP/ $P_{\text{gpdA}}$ -GFP-Atg8 was amplified with primers pairs Ama1-BamHI-gpd-F and TAA-RFP-R/RFP-gpdA-F and Ama1-BamHI-Atg8-R. Next, the two fragments were subcloned into prg3-AMAI-NotI with the One Step Cloning Kit (Vazyme, C113) forming pAMA1- $P_{\text{gpdA}}$ -CpyA-RFP- $P_{\text{gpdA}}$ -GFP-Atg8.

For overexpressing *pmcA*/*pmcB*, plasmid pBARGPE-hph- $P_{\text{gpdA}}$ -*pmcA*/*pmcB* overexpressing *pmcA*/*pmcB* were generated as follows: PCR, using the joint primers ClaI-*pmcA*/*pmcB*-F and ClaI-*pmcA*/*pmcB*-R, were used to generate *pmcA*/*pmcB* fragment that include the complete ORF and 3'UTR of the indicated genes. Next, the three fragments were, respectively, subcloned into the *Cla*I site of the plasmid to generate overexpression plasmids pBARGPE-hph- $P_{\text{gpdA}}$ -*pmcA*/*pmcB*, which contain a selective marker gene *hph* to resist hygromycin.

For amplifying the repair template gfp-hph, the plasmid p-zero-gfp-hph was generated as follows: the selectable marker *hph* was amplified by PCR using the primers HPH-F and HPH-R, and then cloned into the pEASY-Blunt vector, generating a plasmid p-zero-hph. Primers NOTI-gfp-F and NOTI-gfp-R were used to generate a GFP fragment. This fragment was then cloned into the *Not*I site of p-zero-hph to generate p-zero-gfp-hph.

For amplifying the repair template ptrA- $P_{\text{gpdA}}$ /ptrA- $P_{\text{gpdA}}$ -gfp, the plasmid p-zero-ptrA- $P_{\text{gpdA}}$ -gfp was generated as follows: the selectable marker *ptrA*

was amplified by PCR using the primers ptrA-F and ptrA-R, and then cloned into the pEASY-Blunt vector, generating a plasmid p-zero-ptrA. Next, the plasmid was linearized with primer zero-F and zero-R. PCR, using primers zero-PgpdA-F/PgpdA-GFP-F and PgpdA-R/zero-GFP-R, were used to amplify  $P_{\text{gpdA}}$  promoter/gfp fragments. The two fragments were fused with primers zero-PgpdA-F and zero-GFP-R, generating  $P_{\text{gpdA}}$ -gfp fragment. Finally, the fusion fragment was subcloned into the linearizing p-zero-ptrA, yielding the plasmid p-zero-ptrA- $P_{\text{gpdA}}$ -gfp.

For amplifying the repair template hph- $P_{\text{gpdA}}$ , the plasmid p-hph-PgpdA was generated as follows: PCR, using primer NotI-PgpdA-F and NotI-TtrpC-R, was used to amplify *gpdA* promoter ( $P_{\text{gpdA}}$ ). Then, the *gpdA* promoter was ligated into the *Not*I site of p-zero-HPH, generating p-hph-PgpdA.

For expressing the N-terminus (300 aa) of CchA, the plasmid pAMA1- $P_{\text{gpdA}}$ -GFP-CchA<sup>N300</sup> was generated as follows: The  $P_{\text{gpdA}}$ -GFP fragment was obtained by PCR with primers, Ama1-BamHI-gpd-F and CchA-GFP-R from p-zero-ptrA- $P_{\text{gpdA}}$ -gfp; The CchA<sup>N300</sup> fragment containing 900 bp of *cchA* ORF 5' was amplified by PCR with primer CchA-F and Ama1-BamHI-CchA<sup>N300</sup>-R. Then, the two fragments were subcloned into prg3-AMAI-NotI with the One Step Cloning Kit (Vazyme, C113), generating the plasmid pAMA1- $P_{\text{gpdA}}$ -GFP-CchA<sup>N300</sup>.

For live animal bioluminescence imaging, the plasmid pBARGPE-pyr4- $P_{\text{gpdA}}$ -Luc expressing Luciferase was generated as follows: PCR, using the joint primers ClaI-Luc-F and ClaI-Luc-R, were used to generate *luc* (Luciferase gene) ORF. Next, the *Luc* fragments was subcloned into the *Cla*I site of the plasmid pBARGPE-pyr4, yielding pBARGPE-pyr4- $P_{\text{gpdA}}$ -Luc.

All the primers and primer annotations were given in supplementary data Table S2.

### Gene-editing with MMEJ-CRISPR in *A. fumigatus*, transformation and strain verification

For editing the *A. fumigatus* gene, the MMEJ-CRISPR system was used as described in our previous published papers [45,49]. sgRNA targeted to the appropriate site of the target gene was synthesized *in vitro* using the MEGAscript T7 Kit (Life Technologies, AM1333). The corresponding repair template (DNA) with microhomology arms was amplified by PCR. Then, the repair template fragments and sgRNA were cotransformed into a Cas9-expressing *A. fumigatus* recipient strain. The primers and annotations for sgRNAs and repair templates are listed in Table S2. Transformation procedures were performed as previously described.

Transformants were selected in medium lacking uridine or uracil or in the presence of 150  $\mu\text{g ml}^{-1}$  hygromycin B (Sangon) or 0.1  $\mu\text{g ml}^{-1}$  pyrithiamine (Sigma). For the recycling usage of the selectable marker *pyr4*, 1  $\text{mg ml}^{-1}$  5-FOA was used for screening recipient strains. All primers used are listed in the supplementary data Table S2. All transformant isolates were verified by diagnostic PCR analysis using mycelia as the source of DNA. Primers were designed to probe upstream and downstream of the expected cleavage sites as labeled in Figure S1D.

### Microscopy observation

For microscopic observation of hyphae morphology, fresh conidia were inoculated onto sterile glass coverslips overlaid with 1 ml of liquid glucose media with or without 10 mM  $\text{CaCl}_2$ . Strains were cultivated on the coverslips at 37°C for 14 h before observation. The coverslips with hyphae were gently washed with PBS three times. Differential interference contrast (DIC) and green/red fluorescent images of the cells were collected with a Zeiss Axio Imager A1 microscope (Zeiss, Jena, Germany). To observe the fluorescence localization of GFP/RFP-tagged proteins, strains were grown in liquid medium at 37°C with shaking at 200 rpm for indicated time, and then the mycelium pellet sandwiched between the microscope slide and coverslips was observed directly by fluorescence microscopy.

### Measurement of the free $\text{Ca}^{2+}$ concentration ([ $\text{Ca}^{2+}$ ])

Measurement of the free  $\text{Ca}^{2+}$  concentration was performed as described previously with some modifications [40,50]. The strains expressing Aeq/Mt-Aeq/CpyA-Aeq were cultured for 2 days to form fresh spores. The spores were filtered through nylon cloth and washed 10 times in distilled deionized water. One million ( $10^6$ ) spores in 100  $\mu\text{l}$  liquid MM were inoculated into each well of a 96-well microtiter plate (Thermo Fischer). The plate was incubated at 37°C for 24 h. The medium was then removed gently with a pipette, and the cells in each well were washed twice with 150  $\mu\text{l}$  PGM (20 mM PIPES pH 6.7, 50 mM glucose, 1 mM  $\text{MgCl}_2$ ). Aequorin was reconstituted by incubating mycelia in 100  $\mu\text{l}$  PGM containing native coelenterazine (2.5  $\mu\text{M}$ ) (Sigma-Aldrich, C-7001) at 4°C for 4 h in the dark. Then, mycelia were washed twice with 150  $\mu\text{l}$  PGM and allowed to recover to room temperature for 1 h. Luminescence was measured with an LB 960 Microplate Luminometer (Berthold Technologies, Germany),

which was controlled by a dedicated computer running the MikroWin 2000 software. At the 20-s time point of luminescence reading, 10 mM  $\text{CaCl}_2$  was applied as a stimulant. At the end of each experiment, the active aequorin was completely discharged by permeabilizing the cells with 20% (v/v) ethanol in the presence of an excess of calcium (3 M  $\text{CaCl}_2$ ) to determine the total aequorin luminescence of each culture. The conversion of luminescence (relative light units [RLU]) into [ $\text{Ca}^{2+}$ ] was performed with using Excel 2019 software (Microsoft). Input data were converted using the following empirically derived calibration formula:  $\text{pCa} = 0.332588 (-\log k) + 5.5593$ , where k is luminescence (in RLU)  $\text{s}^{-1}$ /total luminescence (in RLU).

### In vitro phosphorylation analysis

GFP-CchA<sup>N300</sup>-expressing *A. fumigatus* were grown in liquid MM for 36 h with shaking at 200 rpm. Then, the mild buffer (10 mM Tris-HCl, pH 7.5, 150 mM NaCl, 0.5 mM EDTA, 0.01% Triton X-100, 1 mM DTT, 1 mM PMSF, and 1:100 protease inhibitor cocktail) was used to extract the total proteins. The GFP-CchA were enriched with a GFP-Trap kit (ChromoTek). After enrichment, samples were separated on 10% SDS-PAGE. The gel bands corresponding to the targeted protein GFP-CchA were excised from the gel. The gel pieces were destained 3 times with 125 mM  $\text{NH}_4\text{HCO}_3$ /50% acetonitrile. Then, proteins were reduced with 10 mM DTT/125 mM  $\text{NH}_4\text{HCO}_3$  at 56°C for 30 min and alkylated with 55 mM iodoacetamide/125 mM  $\text{NH}_4\text{HCO}_3$  for 30 min in the dark. After washing twice with 50% acetonitrile, the gel pieces were dried in a vacuum centrifuge. Then, 200 ng trypsin in 25 mM  $\text{NH}_4\text{HCO}_3$  was added, and the digestion was maintained at 37°C overnight. After digestion, 0.5% formic acid/50% acetonitrile was added to extract peptides from the gel pieces. The extraction procedure was repeated, and the three extracts were combined and dried by vacuum centrifugation. The peptide samples were dissolved in 2% acetonitrile/0.1% formic acid and analyzed using a TripleTOF 5600+ mass spectrometer coupled with the Eksigent nanoLC System (SCIEX, USA). Peptide was loaded onto a C18 trap column (5  $\mu\text{m}$ , 100  $\mu\text{m} \times 20 \text{ mm}$ ) and eluted at 300  $\text{nl min}^{-1}$  onto a C18 analytical column (3  $\mu\text{m}$ , 75  $\mu\text{m} \times 150 \text{ mm}$ ) over a 60-min gradient. The two mobile phases were buffer A (2% acetonitrile/0.1% formic acid/98%  $\text{H}_2\text{O}$ ) and buffer B (98% acetonitrile/0.1% formic acid/2%  $\text{H}_2\text{O}$ ). For information dependent acquisition (IDA), survey scans were acquired in 250 ms, and 40 product ion scans were collected in 50 ms/per scan. MS1 spectra

were collected in the range 350–1500 m/z, and MS2 spectra were collected in the range of 100–1500 m/z. Precursor ions were excluded from reselection for 15 s. Phosphorylation site identification was achieved by searching the obtained MS spectra files using Mascot Daemon software.

### Proteomics

The Proteomics experiment was performed at Hangzhou PTM Biolabs Co., Ltd. as a commercial service. In brief, lysis buffer (8 M urea, 1% Triton-100, 10 mM dithiothreitol, and 1% Protease Inhibitor Cocktail (Calbiochem)) was used to extract the total protein. Proteins were digested with trypsin (Promega) to be peptides and then processed according to the manufacturer's protocol for TMT kit. The labeled tryptic peptides were fractionated by HPLC using a Thermo Betasil C18 column (5  $\mu$ M particles, 10 mm diameter, 250 mm length). After fractioning, the tryptic peptides were analyzed with LC-MS/MS system. The MS/MS data processing was performed using Maxquant search engine (v.1.5.2.8). Tandem mass spectra were searched against *Aspergillus* UniProt database concatenated with reverse decoy database. Proteins with change ratios significantly different from general protein variation ( $\Delta cnaA$ /wild-type > 1.50 or < 0.67) were analyzed for GO terms and KEGG pathway analysis using the UniProt-GOA database (<http://www.ebi.ac.uk/GOA/>) and the KEGG database, respectively.

### Virulence assay

For mouse infection model challenged with *A. fumigatus* conidia, ICR mice (6–8 weeks old, male,  $25 \pm 5$  g) were purchased from Beijing Vital River Laboratory Animal Technology Co., Ltd. The mice were randomized into four groups ( $n = 10$  each). Mice were immunosuppressed on day –3 and –1 with cyclophosphamide (150 mg  $\text{kg}^{-1}$ ) and on day –1 with hydrocortisone acetate (40 mg  $\text{kg}^{-1}$ ). On day 0, mice were anesthetized with 1% pentobarbital sodium (10 ml  $\text{kg}^{-1}$ ) and infected intratracheally with a 50- $\mu$ l slurry containing  $5 \times 10^6$  conidia or 50  $\mu$ l of PBS as the control. Cyclophosphamide (150 mg  $\text{kg}^{-1}$ ) was injected every 3 days after infection to maintain immunosuppression. Survival was monitored two weeks after inoculation. Lung tissue was processed for histology, Grocott's methenamine silver stain and periodic acid-Schiff (PAS) staining were performed. For mouse infection model challenged with *A. fumigatus* hyphae, the mycelia of each strain were homogenized into hyphae fragments using tissue grinding and filtered with lens-

cleaning paper in sterile normal saline. The optical density at 600 nm of the 10-fold dilutions of each group were finally adjusted to 0.5. The ICR mice described as above (4 groups,  $n = 10$  each) were immunosuppressed on day –3 and –1 with cyclophosphamide (150 mg  $\text{kg}^{-1}$ ). On day 0, mice were anesthetized with pentobarbital sodium and then infected intratracheally with a 50- $\mu$ l hyphal suspension. Cyclophosphamide (150 mg  $\text{kg}^{-1}$ ) was injected every 3 days to maintain immunosuppression. Survival was monitored 10 days after inoculation. To directly monitor the infection status in the hyphal infection model, luciferase-expressing *A. fumigatus* strains were used to infect mice, and live mouse bioluminescence imaging was performed. The mice (4 groups,  $n = 5$  each) were immunosuppressed and infected as in the above description. The infected mice were introduced intraperitoneally with 100  $\mu$ l D-luciferin in PBS (33.3 mg  $\text{ml}^{-1}$ ) 10 min before bioluminescence imaging. Mice were anesthetized using 2.5% isoflurane with a constant flow and then placed in an IVIS Lumina XR system chamber. Scanning was performed on day 4. The region was cropped in the chest area from each animal, and the total bioluminescence signal intensity of the lung region was extracted and analyzed using Living Image 4.2 (Caliper Life Sciences).

### Ethics statement

Animal infection experiments were performed following the Guide for the Care and Use of Laboratory Animals of the U.S. National Institutes of Health. The animal experimental protocol was approved by the Animal Care and Use Committee of Nanjing Normal University, China (permit no. LACUC-20,200,703) according to the governmental guidelines for animal care.

### Statistics

Data were given as means  $\pm$  SD. The SD was from at least three biological replicates. Statistical significance was estimated with Graphpad Prism 7 using Student's *t*-test or log-rank test. P-values less than 0.05 were considered statistically significant.

### Discussion

The critical role of calcineurin in calcium dysregulation-related human diseases has been recognized for decades [51]. In fungi, calcineurin has been considered an attractive antifungal target because it is essential for stress survival, development, drug resistance, and



virulence [34]. Previous studies have reported that calcineurin protects *Candida albicans* from toxicity caused by the endogenous levels of calcium in serum [52], which is consistent with our results showing that exogenous calcium is toxic when fungal cells lack functional calcineurin in *A. fumigatus* (Figure 1). These findings suggest that the role of calcineurin in calcium stress survival mechanism is conserved in *Candida* and *Aspergillus* species. However, the underlying mechanism by which calcineurin orchestrates intracellular calcium dynamics remains elusive. Here, through the successful development of an intracellular calcium dynamics monitoring method, we demonstrated that calcineurin dysfunction disturbed calcium homeostasis in the cytosol, vacuole, and mitochondria, leading to a dramatic induction of autophagy and organelle fragmentation and ultimately resulting in significant cell growth inhibition and cell death in the presence of calcium stimuli.

Typically, the resting cytosolic  $\text{Ca}^{2+}$  concentration in *A. fumigatus* ranges from 0.05 to 0.1  $\mu\text{M}$ . In the  $\Delta\text{cnaA}$  mutant, the cytosolic resting  $\text{Ca}^{2+}$  level increased by two-fold compared to that of the wild-type prior to calcium stimuli, which is in line with our previous reports on *A. nidulans*. Moreover, when cells were challenged with 10 mM  $\text{Ca}^{2+}$ , the  $\Delta\text{cnaA}$  mutant displayed a 33% increase in  $[\text{Ca}^{2+}]_c$  amplitude compared to that of the wild-type. These data support the evolutionarily conserved role of calcineurin in maintaining cytosolic calcium homeostasis across fungal species. The sustained increased cytosolic calcium concentration led us to question whether calcium homeostasis in the intracellular calcium stores such as mitochondria and vacuole would be affected by a lack of calcineurin. We established a novel vacuolar  $\text{Ca}^{2+}$  detection approach by fusing the vacuole-targeted protein carboxypeptidase Y (CpyA) to the N-terminus of aequorin, and we found that in the presence of extracellular calcium stimuli, the basal resting level of  $[\text{Ca}^{2+}]_{\text{vac}}$  and the transient  $[\text{Ca}^{2+}]_{\text{vac}}$  in the  $\Delta\text{cnaA}$  mutant were significantly increased, whereas the calcium signature in mitochondria was not significantly affected, implying that vacuoles may be the major site for the detoxification of excess cytosolic calcium in *A. fumigatus*. Collectively, these data demonstrated that calcineurin not only regulates the resting cytosolic calcium but also affects the vacuolar calcium transient response. Importantly, the increased cytosolic resting  $[\text{Ca}^{2+}]_c$  level and the  $[\text{Ca}^{2+}]_{\text{vac}}$  amplitude seen in the  $\Delta\text{cnaA}$  mutant can be suppressed by deleting the calcium channel CchA, suggesting that calcineurin negatively regulates CchA when cells are exposed to calcium. Accordingly, the feedback relationship

between calcineurin and the calcium channel CchA has been described in yeast and *A. nidulans* [44,53]. In yeast, it has been proposed that Cch1 is dephosphorylated by calcineurin *in vitro* [54], leading to the inhibition of calcium channel activity, which is in accord with our phosphoproteomic analysis showing that Serine 55 in CchA could be directly dephosphorylated by calcineurin in *A. fumigatus* (Fig. S8).

In addition to the disordered intracellular calcium homeostasis, the  $\Delta\text{cnaA}$  mutant exhibited the global fragmentation of organelles including the vacuole, the nucleus, ER, and mitochondria, and aggressive autophagy when grown in the presence of 10 mM calcium. Under calcium-treated condition, the growth cessation and cell death of the  $\Delta\text{cnaA}$  mutant start to occur at 60 h and this phenomenon was exacerbated with prolonged incubation time, indicating that the relatively low concentration of calcium is toxic to calcineurin-deficient mutant *A. fumigatus*. It has been well established that the vacuole plays a key role in detoxifying the excess calcium when cells are exposed to external calcium. Thus, we hypothesized that the cytoplasmic calcium excess combined with deficient vacuolar detoxification capacity would give rise to the calcium-toxicity related phenotypes observed in the  $\Delta\text{cnaA}$  mutant. This hypothesis was supported by the fact that alleviating cytosolic calcium overload by the deletion of *cchA* or increasing vacuolar calcium storage capacity by overexpressing of the P-type  $\text{Ca}^{2+}$ -ATPase PmcA can significantly suppress the defective phenotypes of the  $\Delta\text{cnaA}$  mutant. These results highlighted the important roles of calcineurin in mediating calcium homeostasis for fungal survival and the detoxification functions of the vacuoles. Of note, blocking CchA or the overexpression of PmcA is unable to completely suppress the vacuolar fragmentation, aggressive autophagy, and growth cessation in the  $\Delta\text{cnaA}$  mutant in the presence of calcium stimuli, implying that there are other calcium pumps or transporters may also be co-operated with them and involved in the regulation of calcium homeostasis. Probably, examples include the mitochondrial  $\text{Ca}^{2+}$  uniporter McuA, the Golgi-localized P-type  $\text{Ca}^{2+}/\text{Mn}^{2+}$ -ATPase PmrA, and the ER-localized P-type ATPase SpfA [47,55,56], all of which have been demonstrated to be required for mediating calcium homeostasis in response to environmental stresses. In addition, although our results suggested that autophagy triggered by the dysregulation of intracellular calcium homeostasis in the  $\Delta\text{cnaA}$  mutant correlates with cell death because blocking autophagy by *atg2* deletion could slow the cell death progress, we cannot eliminate the possibility that other “toxic factors” affect the viability of *A. fumigatus* calcineurin mutants in the presence of calcium. Proteomic analysis revealed that the

abundance of various peptidases, nucleases, metacaspases CasA and CasB, and autophagy-related proteins were increased in the  $\Delta cnaA$  mutant compared to the wild-type strain in calcium-treated conditions for 60 h, implying that apoptosis/apoptotic-like and/or autophagic cell death may occur. Taken together, these results suggested that the disrupted morphology of organelles and increased expression of cell death-related enzymes contribute to calcium toxicity in *A. fumigatus* calcineurin mutants.

Although cyclosporine A and FK506 (tacrolimus), calcineurin inhibitors, have been shown to possess *in vitro* antifungal activity against fungal pathogens including *A. fumigatus*, *C. albicans*, and *C. neoformans*, the clinical use of calcineurin inhibitors for antifungal therapy remains limited due to their immunosuppressive side effects [19,37,57]. Because calcineurin inhibitors exhibit synergistic fungicidal activity with antifungal drugs, research on analogues of calcineurin inhibitors with antifungal activity but low immunosuppressive properties may be a promising direction. Encouragingly, APX879, the FK506 analogue, has been shown to exhibit reduced immunosuppressive activity while maintaining limited antifungal activity against pathogens in a murine infection model [58]. Our findings showing that exogenous calcium is able to significantly inhibit the growth of calcineurin mutants highlights a possibility that the combination of calcium and nonimmunosuppressive calcineurin inhibitors could enhance therapeutic efficacy against human pathogens.

## Acknowledgments

This work was financially supported by National Key Research and Development Program of China (2019YFA0904900), National Natural Science Foundation of China (31861133014 and 31770086), Program for Jiangsu Excellent Scientific and Technological Innovation team (17CXTD00014), Priority Academic Program Development of Jiangsu Higher Education Institutions to L.L. National Natural Science Foundation of China (31900404) and National Science Foundation of the Jiangsu Higher Education Institutions of China (19KJB180017) to Y.Z. We thank Gustavo H. Goldman (University of São Paulo) for kindly providing helpful comments on the manuscript.

## Funding

This work was supported by the National Key Research and Development Program of China (2019YFA0904900); National Natural Science Foundation of China [31861133014]; National Natural Science Foundation of China [31770086]; National Natural Science Foundation of China [31900404]; National Science Foundation of the Jiangsu

Higher Education Institutions of China [19KJB180017]; Priority Academic Program Development of Jiangsu Higher Education Institutions; Program for Jiangsu Excellent Scientific and Technological Innovation Team [17CXTD00014].

## Author contributions

C.Z., Y.Z. and L.L., conceived the study; C.Z., Y.R., H.G., and L.G. performed the experiments; and C.Z., Y.Z. and L. L. analyzed and interpreted the data and wrote the manuscript with input from all authors.

## Disclosure statement

No potential conflict of interest was reported by the authors.

## ORCID

Yuanwei Zhang  <http://orcid.org/0000-0003-0854-6123>

Ling Lu  <http://orcid.org/0000-0002-2891-7326>

## References

- [1] Islam MS. Calcium signaling: from basic to bedside. *Adv Exp Med Biol.* 2020;1131:1–6.
- [2] Rosendo-Pineda MJ, Moreno CM, Vaca L. Role of ion channels during cell division. *Cell Calcium.* 2020;91:102258.
- [3] Carafoli E. Intracellular calcium homeostasis. *Annu Rev Biochem.* 1987;56(1):395–433.
- [4] Cyert MS, Philpott CC. Regulation of cation balance in *Saccharomyces cerevisiae*. *Genetics.* 2013;193:677–713.
- [5] Blatzer M, Latge JP. Metal-homeostasis in the pathobiology of the opportunistic human fungal pathogen *Aspergillus fumigatus*. *Cur Opin Microbiol.* 2017;40:152–159.
- [6] Park HS, Lee SC, Cardenas ME, et al. Calcium-Calmodulin-Calcineurin signaling: a globally conserved virulence cascade in eukaryotic microbial pathogens. *Cell Host Microbe.* 2019;26(4):453–462.
- [7] Thewes S. Calcineurin-Crz1 signaling in lower eukaryotes. *Eukaryot Cell.* 2014;13(6):694–705.
- [8] Cunningham KW. Acidic calcium stores of *Saccharomyces cerevisiae*. *Cell Calcium.* 2011;50(2):129–1238.
- [9] Miseta A, Fu L, Kellermayer R, et al. The golgi apparatus plays a significant role in the maintenance of  $Ca^{2+}$  Homeostasis in the vps33 $\Delta$  Vacuolar biogenesis mutant of *Saccharomyces cerevisiae*. *J Biol Chem.* 1999a;274(9):5939–5947.
- [10] Miseta A, Kellermayer R, Aiello DP, et al. The vacuolar  $Ca^{2+}/H^{+}$  exchanger Vcx1p/Hum1p tightly controls cytosolic  $Ca^{2+}$  levels in *S. cerevisiae*. *FEBS Lett.* 1999b;451(2):132–136.
- [11] Munoz A, Chu M, Marris PI, et al. Specific domains of plant defensins differentially disrupt colony initiation, cell fusion and calcium homeostasis in *Neurospora crassa*. *Mol Microbiol.* 2014;92(6):1357–1374.

- [12] Dolgin E. How secret conversations inside cells are transforming biology. *Nature*. 2019;567(7747):162–164.
- [13] La Rovere RM, Roest G, Bultynck G, et al. Intracellular Ca<sup>2+</sup> signaling and Ca<sup>2+</sup> microdomains in the control of cell survival, apoptosis and autophagy. *Cell Calcium*. 2016;60:74–87.
- [14] Dunn T, Gable K, Beeler T. Regulation of cellular Ca<sup>2+</sup> by yeast vacuoles. *J Cell Biol*. 1994;269:7273–7278.
- [15] Forster C, Kane PM. Cytosolic Ca<sup>2+</sup> homeostasis is a constitutive function of the V-ATPase in *Saccharomyces cerevisiae*. *J Biol Chem*. 2000;275(49):38245–38253.
- [16] Kmetzsch L, Staats CC, Simon E, et al. The vacuolar Ca<sup>2+</sup> exchanger Vcx1 is involved in Calcineurin-Dependent Ca<sup>2+</sup> Tolerance and virulence in *Cryptococcus neoformans*. *Eukaryot Cell*. 2010a;9(11):1798–1805.
- [17] Chang Y, Schlenstedt G, Flockerzi V, et al. Properties of the intracellular transient receptor potential (TRP) channel in yeast, Yvc1. *FEBS Lett*. 2010;584(10):2028–2032.
- [18] Denis V, Cyert MS. Internal Ca<sup>2+</sup> release in yeast is triggered by hypertonic shock and mediated by a TRP channel homologue. *J Cell Biol*. 2002;156(1):29–34.
- [19] Hamamoto S, Mori Y, Yabe I, et al. In vitro and in vivo characterization of modulation of the vacuolar cation channel TRPY 1 from *Saccharomyces cerevisiae*. *Febs J*. 2018;285(6):1146–1161.
- [20] Lange I, Yamamoto S, Partida-Sanchez S, et al. TRPM<sup>2+</sup> functions as a lysosomal Ca<sup>2+</sup>-release channel in beta cells. *Sci Signal*. 2009; (71):2. 10.1126/scisignal.2000278.
- [21] Yu Q, Wang F, Zhao Q, et al. A novel role of the vacuolar calcium channel Yvc1 in stress response, morphogenesis and pathogenicity of candida albicans. *Int J Med Microbiol*. 2014;304(3–4):339–350.
- [22] Cunningham KW, Fink GR. Calcineurin inhibits VCX1-dependent H<sup>+</sup>/Ca<sup>2+</sup> exchange and induces Ca<sup>2+</sup> ATPases in *Saccharomyces cerevisiae*. *Mol Cell Biol*. 1996;16(5):2226–2237.
- [23] Dinamarco TM, Freitas FZ, Almeida RS, et al. Functional characterization of an *Aspergillus fumigatus* calcium transporter (PmcA) that is essential for fungal infection. *PLoS One*. 2012;7(5):e37591.
- [24] Ferreira RT, Silva ARC, Pimentel C, et al. Arsenic stress elicits cytosolic Ca<sup>2+</sup> bursts and Crz1 activation in *Saccharomyces cerevisiae*. *Microbiology-Sgm*. 2012;158(9):2293–2302.
- [25] Kmetzsch L, Staats CC, Simon E, et al. The vacuolar Ca<sup>2+</sup> exchanger Vcx1 is involved in calcineurin-dependent Ca<sup>2+</sup> tolerance and virulence in *Cryptococcus neoformans*. *Eukaryot Cell*. 2010b;9(11):1798–1805.
- [26] Klionsky DJ. Cell biology – Autophagy as a regulated pathway of cellular degradation. *Science*. 2000;290(5497):1717–1721.
- [27] Nakatogawa H. Mechanisms governing autophagosome biogenesis. *Nat RevMol Cell Biol*. 2020;21:439–458.
- [28] Liu R, Li J, Zhang T, et al. Itraconazole suppresses the growth of glioblastoma through induction of autophagy: involvement of abnormal cholesterol trafficking. *Autophagy*. 2014;10(7):1241–1255.
- [29] Wang Y, Zhang H. Regulation of autophagy by mTOR signaling pathway. *Adv Exp Med Biol*. 2019;1206:67–83.
- [30] Yi C, Tong JJ, Yu L. Mitochondria: the hub of energy deprivation-induced autophagy. *Autophagy*. 2018;14:1084–1085.
- [31] Scarlatti F, Granata R, Meijer AJ, et al. Does autophagy have a license to kill mammalian cells?. *Cell Death Differ*. 2009;16(1):12–20.
- [32] White E, DiPaola RS. The double-edged sword of autophagy modulation in cancer. *Clin Cancer Res*. 2009;15(17):5308–5316.
- [33] Denning DW, Bromley MJ. Infectious disease. How to bolster the antifungal pipeline. *Science*. 2015;347(6229):1414–1416.
- [34] Juvvadi PR, Lee SC, Heitman J, et al. Calcineurin in fungal virulence and drug resistance: prospects for harnessing targeted inhibition of calcineurin for an antifungal therapeutic approach. *Virulence*. 2017;8(2):186–197.
- [35] Steinbach WJ, Cramer RA Jr., Perfect BZ, et al. Calcineurin controls growth, morphology, and pathogenicity in *Aspergillus fumigatus*. *Eukaryot Cell*. 2006;5(7):1091–1103.
- [36] Steinbach WJ, Cramer RA Jr., Perfect BZ, et al. Calcineurin inhibition or mutation enhances cell wall inhibitors against *Aspergillus fumigatus*. *Antimicrob Agents Chemother*. 2007;51(8):2979–2981.
- [37] Fox DS, Heitman J. Good fungi gone bad: the corruption of calcineurin. *Bioessays*. 2002;24(10):894–903.
- [38] Park HS, Chow EW, Fu C, et al. Calcineurin targets involved in stress survival and fungal virulence. *PLoS Pathog*. 2016;12(9):e1005873.
- [39] Juvvadi PR, Fortwendel JR, Rogg LE, et al. Localization and activity of the calcineurin catalytic and regulatory subunit complex at the septum is essential for hyphal elongation and proper septation in *aspergillus fumigatus*. *Mol Microbiol*. 2011;82(5):1235–1259.
- [40] Nelson G, Kozlova-Zwinderman O, Collis AJ, et al. Calcium measurement in living filamentous fungi expressing codon-optimized aequorin. *Mol Microbiol*. 2004;52(5):1437–1550.
- [41] Kikuma T, Ohneda M, Arioka M, et al. Functional analysis of the ATG8 homologue Aotg8 and role of autophagy in differentiation and germination in *Aspergillus oryzae*. *Eukaryot Cell*. 2006;5(8):1328–1336.
- [42] Kotani T, Kirisako H, Koizumi M, et al. The Atg2-Atg18 complex tethers pre-autophagosomal membranes to the endoplasmic reticulum for autophagosome formation. *Proc Natl Acad Sci U S A*. 2018;115(41):10363–10368.
- [43] Tang Z, Takahashi Y, Wang HG. ATG2 regulation of phagophore expansion at mitochondria-associated ER membranes. *Autophagy*. 2019;15(12):2165–2166.
- [44] Wang S, Liu X, Qian H, et al. Calcineurin and Calcium channel CchA coordinate the salt stress response by regulating Cytoplasmic Ca<sup>2+</sup> Homeostasis in *Aspergillus nidulans*. *Appl Environ Microbiol*. 2016;82(11):3420–3430.
- [45] Zhang C, Lu L. Precise and efficient in-frame integration of an exogenous GFP tag in *Aspergillus fumigatus* by a CRISPR system. *Methods Mol Biol*. 2017;1625:249–258.

- [46] Greene V, Cao H, Schanne FA, et al. Oxidative stress-induced calcium signalling in *Aspergillus nidulans*. *Cell Signaling*. 2002;14(5):437–443.
- [47] Song J, Liu X, Zhai P, et al. A putative mitochondrial calcium uniporter in *A. fumigatus* contributes to mitochondrial  $\text{Ca}^{2+}$  homeostasis and stress responses. *Fungal Genet Biol*. 2016a;94:15–22.
- [48] Song J, Zhai P, Zhang Y, et al. The aspergillus fumigatus damage resistance protein family coordinately regulates ergosterol biosynthesis and azole susceptibility. *mBio*. 2016b;7(1):e01919–01915.
- [49] Zhang C, Meng XH, Wei XL, et al. Highly efficient CRISPR mutagenesis by microhomology-mediated end joining in *Aspergillus fumigatus*. *Fungal Genet Biol*. 2016a;86:47–57.
- [50] Zhang Y, Zheng Q, Sun C, et al. Palmitoylation of the Cysteine residue in the DHHC Motif of a Palmitoyl Transferase Mediates  $\text{Ca}^{2+}$  Homeostasis in *Aspergillus*. *PLoS Genet*. 2016b;12(4):e1005977.
- [51] Park YJ, Yoo SA, Kim M, et al. The role of Calcium-Calcineurin-NFAT signaling pathway in health and autoimmune diseases. *Front Immunol*. 2020;11:195.
- [52] Blankenship JR, Heitman J. Calcineurin is required for *Candida albicans* to survive calcium stress in serum. *Infect Immun*. 2005;73(9):5767–5774.
- [53] Ma Y, Sugiura R, Koike A, et al. Transient receptor potential (TRP) and Cch1-Yam8 channels play key roles in the regulation of cytoplasmic  $\text{Ca}^{2+}$  in fission yeast. *PLoS One*. 2011;6(7):e22421.
- [54] Bonilla M, Cunningham KW. Mitogen-activated Protein Kinase Stimulation of  $\text{Ca}^{2+}$  Signaling is required for survival of endoplasmic reticulum stress in yeast. *Mol Biol Cell*. 2003;14(10):4296–4305.
- [55] Pinchai N, Juvvadi PR, Fortwendel JR, et al. The *Aspergillus fumigatus* P-type Golgi apparatus  $\text{Ca}^{2+}/\text{Mn}^{2+}$  ATPase PmrA is involved in cation homeostasis and cell wall integrity but is not essential for pathogenesis. *Eukaryot Cell*. 2010;9(3):472–476.
- [56] Yu Q, Wang H, Xu N, et al. Spf1 strongly influences calcium homeostasis, hyphal development, biofilm formation and virulence in *Candida albicans*. *Microbiology*. 2012;158(9):2272–2282.
- [57] Groll AH, De Lucca AJ, Walsh TJ. Emerging targets for the development of novel antifungal therapeutics. *Trends Microbiol*. 1998;6(3):117–124.
- [58] Juvvadi PR, Fox D 3rd, Bobay BG, et al. Harnessing calcineurin-FK506-FKBP12 crystal structures from invasive fungal pathogens to develop antifungal agents. *Nature Commun*. 2019;10(1):4275.